catalysts

MDPI

Article

Alkene Epoxidation and Thioether Oxidation with Hydrogen Peroxide Catalyzed by Mesoporous Zirconium-Silicates

Irina D. Ivanchikova [1], Olga V. Zalomaeva [1], Nataliya V. Maksimchuk [1], Olga A. Stonkus [1], Tatiana S. Glazneva [1], Yurii A. Chesalov [1], Alexander N. Shmakov [1], Matteo Guidotti [2] and Oxana A. Kholdeeva [1,*]

[1] Boreskov Institute of Catalysis, Lavrentieva Ave. 5, Novosibirsk 630090, Russia; idi@catalysis.ru (I.D.I.); zalomaeva@catalysis.ru (O.V.Z.); nvmax@catalysis.ru (N.V.M.); stonkus@catalysis.ru (O.A.S.); glazn@catalysis.ru (T.S.G.); chesalov@catalysis.ru (Y.A.C.); shurka@catalysis.ru (A.N.S.)
[2] CNR-SCITEC, Via C. Golgi 19, 20133 Milano, Italy; matteo.guidotti@scitec.cnr.it
* Correspondence: khold@catalysis.ru

Abstract: Mesoporous zirconium-silicates have been prepared using two different methodologies, evaporation-induced self-assembly and solventless organometallic precursor dry impregnation of commercial SiO_2. The samples were characterized by elemental analysis, XRD, N_2 adsorption, TEM, DRS UV–vis and Raman spectroscopic techniques. The catalytic performance of the Zr-Si catalysts was assessed in the epoxidation of three representative alkenes, cyclohexene, cyclooctene and caryophyllene, as well as in the oxidation of methyl phenyl sulfide using aqueous hydrogen peroxide as a green oxidant, with special attention drawn to the structure/activity relationship and catalyst stability issues. The key factors which affect substrate conversion and epoxide selectivity have been defined. The catalysts with larger contents of oligomeric ZrO_2 species revealed higher activity. The nature of alkene and, in particular, its molecular hindrance is crucial, since the adsorption of the epoxide product is the main factor leading to fast catalyst deactivation. In fact, bulky epoxides do not show this effect. After optimization, the oxidation of caryophyllene gave endocyclic monoepoxide with 77% selectivity at 87% alkene conversion. Methyl phenyl sulfoxide afforded 37% of sulfoxide and 63% of sulfone at 57% sulfide conversion. The nature of catalysis was truly heterogeneous and no Zr leaching was observed.

Keywords: alkene; epoxidation; evaporation–induced self–assembly; heterogeneous catalysis; hydrogen peroxide; mesoporous zirconium–silicate

Citation: Ivanchikova, I.D.; Zalomaeva, O.V.; Maksimchuk, N.V.; Stonkus, O.A.; Glazneva, T.S.; Chesalov, Y.A.; Shmakov, A.N.; Guidotti, M.; Kholdeeva, O.A. Alkene Epoxidation and Thioether Oxidation with Hydrogen Peroxide Catalyzed by Mesoporous Zirconium-Silicates. *Catalysts* **2022**, *12*, 742. https://doi.org/10.3390/catal12070742

Academic Editors: Sébastien Leveneur, Vincenzo Russo and Pasi Tolvanen

Received: 14 June 2022
Accepted: 3 July 2022
Published: 5 July 2022

1. Introduction

Epoxides are key intermediates in the production of a wide variety of valuable products [1]. The selective epoxidation of alkenes with the green oxidant hydrogen peroxide using heterogeneous catalysts is an environmentally benign and economically sound route for the synthesis of epoxides and their derivatives [2–6]. Impressive progress has been made in this area due to the development of titanium silicalite-1 (TS-1) by the Eni group and its implementation for propene epoxidation [7,8]. However, the small pore size of TS-1 (ca. 5.5 Å) does not allow for transformation of bulky alkene substrates. Such limitation stimulated further research activity in the synthesis of mesoporous metal-silicates and the assessment of their catalytic performance started in the mid-1990s [9–12].

Significant advances have been achieved in the incorporation of Ti, Zr, Nb, W and some other transition metals into mesoporous silica matrixes using various synthetic methodologies [13–18]. Following the noteworthy success of TS-1, mesoporous titanium-silicates have received the greatest attention [9–14,19–27]. However, several research groups demonstrated that Nb-silicates can be more efficient than Ti-ones in the epoxidation of bulky alkenes with H_2O_2 and, moreover, possess better stability than the latter [28–34]. Some success has been recorded in the preparation of tungsten-containing silicates

and their use in oxidation catalysis; however, partial tungsten leaching under the conditions of liquid-phase oxidation with H_2O_2 still remains an unresolved problem [35–41].

Although first attempts to insert zirconium into silica matrixes date back to the late 1990s [42–44], oxidation catalysis over Zr-silicates remains largely underexplored [42,43,45–50]. Oxidation of aniline and alkylphenols/naphthols were among the most studied reactions, while oxidation of alkenes and thioethers was less investigated, especially from the viewpoint of the oxidation mechanism. Strukul and co-workers revealed that ZrO_2-SiO_2 mixed oxides prepared by sol-gel method could accomplish oxidation of cyclooctene and cyclohexene to give corresponding diols as the main oxidation products [45,46]. In turn, Maksimchuk et al. demonstrated that Zr-MCF prepared by impregnation of the mesostructured silica support with Zr(IV) isopropoxide is an efficient catalyst for the allylic oxidation of α-pinene [47]. On the other hand, Zr-SiO_2 made through a molecular precursor method showed very low activity in both alkene and thioether oxidation [33,51]. Meanwhile, more recent works on Zr-substituted polyoxometalates (Zr-POM) [52] and Zr-based metal-organic frameworks (Zr-MOF) [53,54] proved that Zr-catalysts can serve as highly effective epoxidation catalysts. These recent findings have stimulated our interest in oxidation catalysis with Zr(IV).

In the present work, we developed unprecedented protocols for the synthesis of leaching-resistant mesoporous Zr-silicates and investigated their catalytic performance in H_2O_2-based oxidation of a few representative olefins and thioethers. Two different methodologies were employed for the catalyst synthesis, namely, evaporation-induced self-assembly (EISA) and solventless dry impregnation of an organometallic Zr precursor onto a commercial mesoporous SiO_2 (OM-DI). Previously, the EISA approach was successfully used for insertion of Ti [27], Nb [32], and W [40] into silicate materials while the OM-DI strategy found application in the preparation of solid oxidic catalysts containing Mo [55,56], Ti and Nb [30,57]. Our present work demonstrated that, regardless of the catalyst preparation method, mesoporous Zr-silicates enable fairly good substrate conversions and product selectivity in the oxidation of bulky alkenes and thioethers. Their common drawback is a fast deactivation caused by the strong adsorption of the epoxide product on Zr active sites. This problem does not exist if bulky alkene molecules are involved in the oxidation process.

2. Results and Discussion

2.1. Synthesis and characterization of Zr-Si-Catalysts

Zirconium is an oxophilic transition metal highly prone to the formation of di(oligo)meric forms [58]. Acetylacetone has been widely employed as a hydrolysis/oligomerization-retarding additive in the sol–gel and template syntheses of mesoporous metal-silicates [13,14,59]. Use of this chelating agent in the EISA-based synthesis of Ti–MMM–E catalysts not only prevented the formation of anatase-like aggregates, but also assisted the generation of a specific, di(oligo)meric state of Ti centers within the silica matrix [27]. The same chelating ligand was successfully employed for the stabilization of Nb and W precursors in the synthesis of Nb–MMM–E and W–MMM–E, respectively, using the EISA methodology [32,40]. In this work, we have extended this approach to the synthesis of mesoporous zirconium-silicates, hereinafter designated as Zr-MMM-E (see Experimental section for details).

Sample **A** was, therefore, prepared by a procedure similar to the one reported earlier for the synthesis of Ti–MMM–E [27], Nb-MMM-E [32] and W-MMM-E [40]. $Zr(acac)_4$ was taken as a zirconium source. The molar ratio of Zr/Si was 0.9/50. For the preparation of samples **B, C**, and **D** we used an increased amount of HCl, corresponding to 1, 2 and 7 equiv of acid to Zr, respectively.

Upon evaporation of ethanol, the critical micelle concentration was achieved and self–assembly of a silica–Zr–surfactant mesophase occurred, resulting in the formation of transparent monoliths. After calcination and grounding, the solids gave a fine white

powder. According to the EISA methodology, the composition of the starting mixtures is replicated in the composition of the resulting materials, as confirmed by the elemental analysis data reported in Table 1.

Table 1. Elemental analysis data and textural characteristics of Zr-silicates.

Catalyst	Zr, [a] wt%	Zr(acac)$_4$:HCl [b]	S_{BET}, m^2/g	V_p, [c] cm^3/g	D_p, [d] nm
A	2.46	1:0	995	0.62	3.8
B	2.33	1:1	1318	0.61	3.6
C	2.43	1:2	1376	0.58	3.5
D	2.50	1:7	1404	0.62	3.1
Zr/SiO$_2$	1.91	- [e]	408	0.66	2.0–8.0 [f]

[a] Based on elemental analysis data for calcined samples. [b] Molar ratio of Zr(acac)$_4$ and extra HCl. [c] Mesopore volume. [d] Average pore diameter. [e] Zirconium was introduced as $Zr(Cp)_2Cl_2$ precursor. [f] Broad distribution of mesopores with a maximum at 4.9 nm.

The textural properties of all Zr-MMM-E samples acquired from the nitrogen adsorption measurements are presented in Table 1, while the nitrogen adsorption-desorption isotherms for samples **A** and **D** are presented in Figure 1. All solids possess mostly mesopores. The increase in the HCl amount added during the synthesis led to the increase in specific BET surface area from 995 m^2/g for sample **A** to 1404 m^2/g for sample **D**. At the same time, the average pore diameter diminished from 3.8 nm for sample **A** to 3.1 nm for sample **D**. Moreover, the mesopore volume did not change significantly and remained in the interval of 0.58–0.62 cm^3/g.

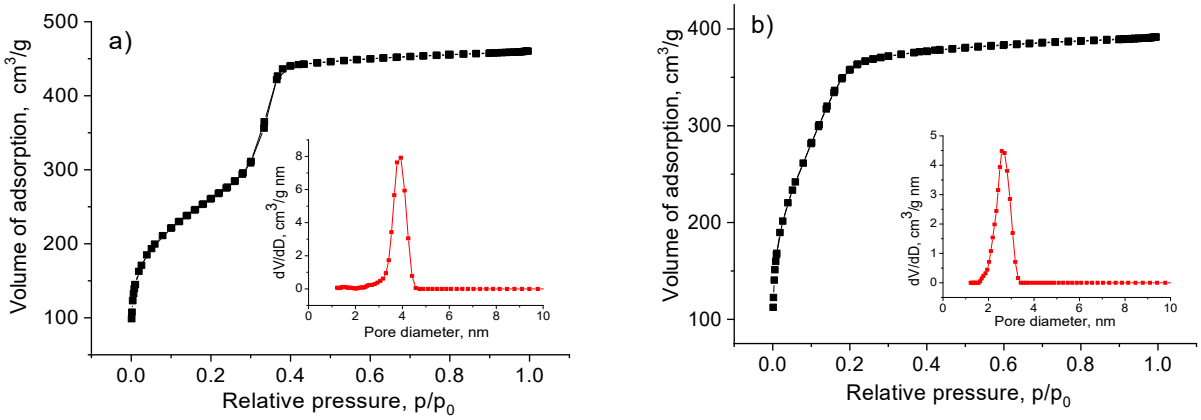

Figure 1. Nitrogen adsorption–desorption isotherm and pore size distribution (inset) for Zr-EISA (**a**) sample **A** and (**b**) sample **D**.

In Table 1, elemental analysis and textural data are also reported for a Zr/SiO$_2$ catalyst that was prepared for the sake of comparison following the organometallic dry impregnation technique (OM-DI). In fact, analogous Ti(IV) and Nb(V) catalysts obtained by impregnating titanocene or niobocene dichloride, respectively, over a commercial non-ordered mesoporous silica support, under solventless conditions, proved to be efficient epoxidation catalysts in the liquid-phase epoxidation of unsaturated terpenes and fatty acid methyl esters [30,57].

While the Zr/SiO$_2$ catalyst is fully amorphous and non-ordered to X-ray analysis, small angle XRD patterns of Zr-MMM-E exhibit a broad diffraction peak around 1.9 and 2.9 2θ° for samples **A** and **D**, respectively (Figure 2), indicating a long–range structural order of cylindrical mesopores typical of EISA-prepared metal-silicates [27,32,40]. No peaks were detected in the wide-angle range, which implies the absence of a zirconium oxide phase in the samples.

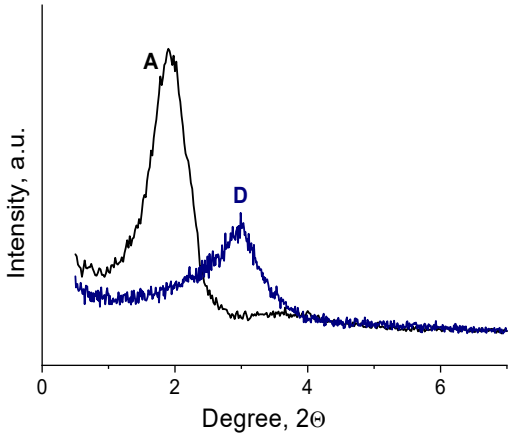

Figure 2. Representative XRD patterns of calcined Zr-MMM-E (samples **A** and **D**).

DR UV–vis spectra of the Zr–MMM–E and Zr/SiO_2 catalysts are shown in Figure 3. Sample **A** synthesized without additional HCl revealed a sharp band with a maximum at 205–210 nm, that is usually attributed in the literature to the ligand-to-metal charge transfer from O^{2-} to Zr^{4+} ion isolated in a silica matrix [44,60–64]. On the contrary, the spectrum of sample **D** prepared with additional 7 equiv of HCl displays a broad absorption in the range of 240–280 nm with a maximum centered at 250–270 nm, which can be assigned to nanoscopic regions of Zr-O-Zr linkages (ZrO_2-like domains) [44,61,64]. The other two materials obtained with 1 and 2 equiv of HCl exhibit both adsorptions, although at a different ratio. It is also worth noting a small shoulder at 220 nm in the spectra of samples **B** and **C**, which can be attributed to small Zr-O-Zr clusters (oligomers) [44,62]. In general, the more amount of HCl added during the synthesis, the higher contribution of oligo(poly)meric ZrO_2 species and their size. The Zr/SiO_2 sample prepared by dry impregnation of silica exhibited a DRS-UV band with a maximum at ca. 210 nm and a shoulder around 240–270 nm (Figure 3), indicating the large occurrence of quasi isolated Zr(IV) species on the silica surface.

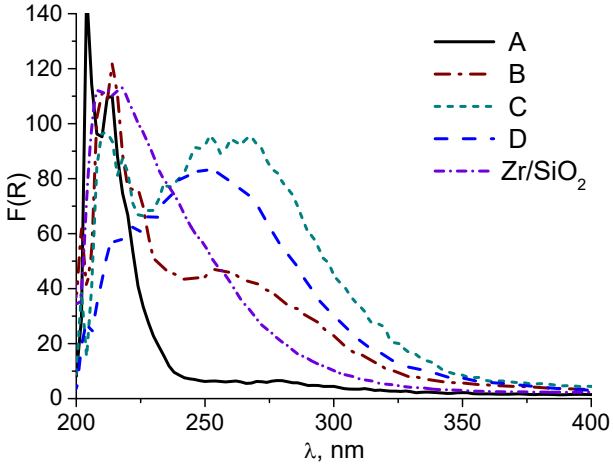

Figure 3. DR UV–vis spectra of Zr–MMM–E (samples **A**–**D**) and Zr/SiO_2.

Raman spectroscopy was also used to investigate the nature of Zr species formed on the catalyst surface. The spectra of samples **A** and **D** are shown in Figure 4 in comparison with the spectra of the zirconium-free silicate matrix. Despite the pronounced difference observed in the DR–UV spectra, all Raman spectra look quite similar. Although the spectra are not well defined, we may conclude that ZrO_2 is present in amorphous and/or clusterized forms rather than in crystalline domains, as no characteristic bands typically

attributed to monoclinic, tetragonal, or cubic modifications of ZrO_2 can be distinguished in the Raman spectra of the Zr-MMM-E samples [65,66].

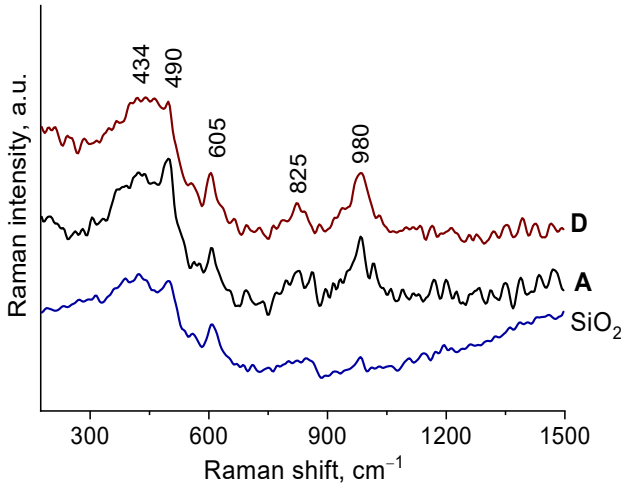

Figure 4. Raman spectra of Zr-EISA samples **A** and **D** in comparison with the Zr-free SiO_2-EISA matrix.

Figure 5 shows TEM and HAADF-STEM images of silicate particles in **A** and **D** samples. The particle size varies over a wide range, from tens of nanometers to several micrometers. According to the EDX-mapping data, a homogeneous distribution of Si and Zr is observed in both samples regardless of the silicate particle size. Quantification gives an atomic ratio Si/Zr ≈ 98.5/1.5 in the studied areas which agrees well with the elemental analysis data.

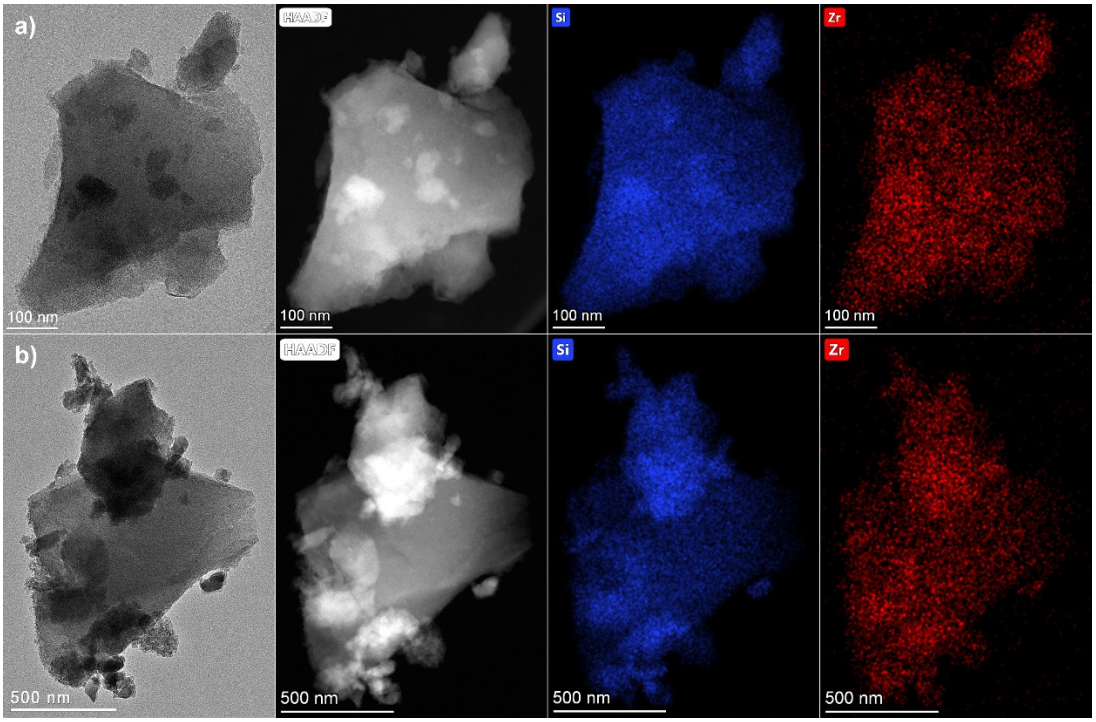

Figure 5. TEM data for samples **A** (**a**) and **D** (**b**): TEM-images, HAADF-STEM images and corresponding EDX-mapping patterns showing distribution of Si (blue) and Zr (red) in selected regions.

The study of the Zr-catalysts in the HAADF-STEM mode allowed us to identify the location of Zr atoms, thanks to their high contrast (Z-contrast). On the HAADF-STEM

image of sample **A** (Figure 6a) one can clearly see the individual bright dots and groups of bright dots with a higher contrast against the background of silicate. These data indicate the presence of Zr in a highly dispersed state. No periodic structures are observed in these areas, indicating the absence of nanoparticles with a defined structure of zirconium oxides. Thus, the zirconium species have a disordered or amorphous structure. A similar state of zirconium was observed in sample **D**. The HRTEM image of this solid (Figure 6b) shows only the amorphous structure of the silicate, while the HAADF-STEM image (inset of Figure 6b) exhibits inhomogeneous contrast indicating the presence of highly dispersed Zr-species.

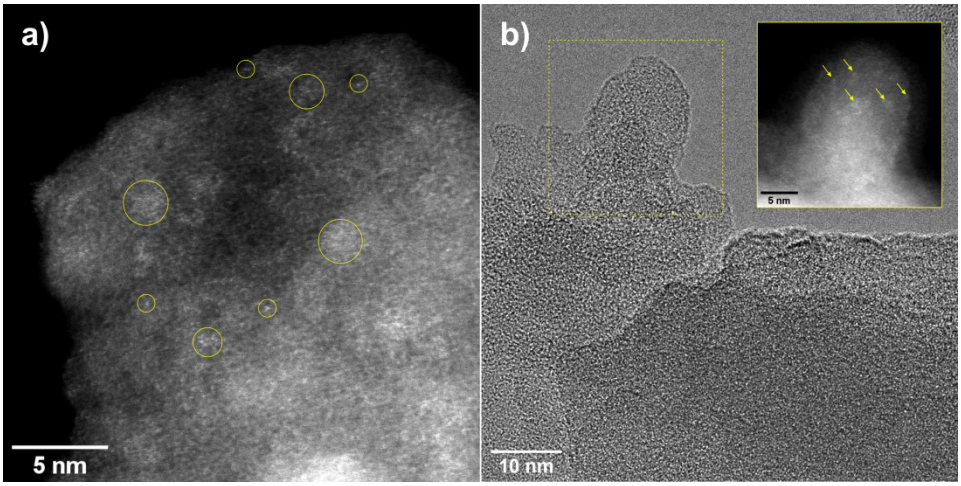

Figure 6. (**a**) HAADF-STEM image of sample **A**; (**b**) HRTEM image of sample **D** and HAADF-STEM image of the marked region shown in inset. The marks on HAADF-STEM images indicate the location of highly dispersed Zr-species.

The acidic and basic properties of the samples were studied using FTIR spectroscopy of the adsorbed probe molecules: carbon monoxide and deuterochloroform. FTIR spectra of calcined samples show a broad high-intensity band with a maximum at 3740 cm^{-1} in the absorption region of OH groups (Figure 7a). This band is usually observed for silicon oxide and indicates isolated Si-OH groups with stretching vibrations at 3740 cm^{-1} [67,68]. In addition, various types of Zr-OH groups with characteristic bands at 3670–3680 and 3760–3780 cm^{-1}, usually observed for ZrO_2, can contribute to such absorption band [69–71]. In this case, the absorption band at 3740 cm^{-1} cannot be separated into contributions from OH groups of various types. However, the presence of different types of OH groups is manifested in differential FTIR spectra by shifts in the absorption bands of the hydroxyl groups during CO adsorption (Figure 7b).

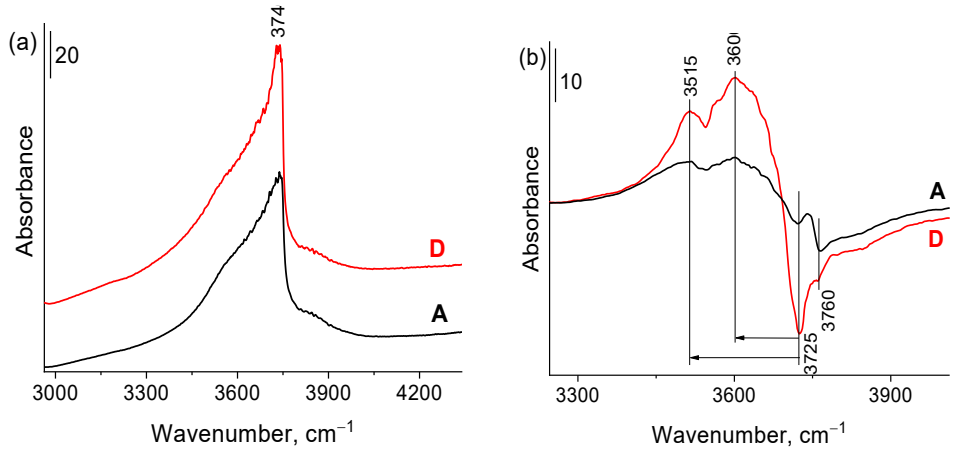

Figure 7. (**a**) FTIR spectra of samples **A** and **D** at room temperature in the absorption region of hydroxyl groups and (**b**) differential FTIR spectra of OH groups after CO adsorption on samples **A** and **D**.

When CO is adsorbed (Figure 7b), the bands at 3725 and 3760 cm^{-1}, characterizing various OH groups, disappear, and broad absorption bands at 3515 and 3600 cm^{-1} are formed, corresponding to hydrogen-bonded complexes of OH groups with CO molecules. Thus, the formation of various types of CO complexes with OH groups differing in strength is clearly seen. The strength of the OH groups (Brønsted acid sites, BAS) was characterized by proton affinity calculated from FTIR spectra using the values of the band shifts [72]. The OH groups characterized by the absorption band at 3760 cm^{-1} belong to Zr^{4+}–OH and do not have pronounced acidic properties [70]. The band at 3725 cm^{-1} is formed by OH groups of two types with a band shift of 125 and 210 cm^{-1}, which corresponds to proton affinities of 1330 and 1230 kJ/mol, respectively. The BAS of silicon dioxide and titanium silicates are known to have very low acidity—the characteristic shifts of the OH group bands are 90–120 cm^{-1} [72–74]. In our case, the BAS strength is much higher, which may be due to the formation of Si-O-Zr bonds and an increase in the electron density on the bridging oxygen. Yamaguchi et al. [75] studied ZrO_2/SiO_2 samples prepared by impregnating SiO_2 with a Zr(*n*-OC_3H_7) solution and also showed an increase in Brønsted acidity due to charge transfer from the ZrO_4 tetrahedron to SiO_4 and strengthening of the Si–O bond. A rise in Brønsted acidity was previously shown for a number of mesoporous silicates modified with zirconium [76–79], which was associated with the introduction of Zr^{4+} ion into the silicate framework resulting in weakening the Si-OZrO–H bond and increasing the acidity of these OH groups.

CO adsorption on two types of BAS can also be observed in the range of carbonyl vibrations (Figure 8): at low CO pressures, there is a band at 2162 cm^{-1}, and with increasing CO pressure, an additional band appears at 2155 cm^{-1}, characterizing CO adsorbed on SiOH groups [53,72,80]. In addition, a band at 2182 cm^{-1} is observed in the spectra, which refers to the adsorption of CO on zirconium cations Zr^{4+} (Lewis acid sites, LAS) [53,70]. The absorption band at 2135 cm^{-1} characterizes the vibrations of physically adsorbed CO [72]. The BAS and LAS concentrations were determined from the integral intensities of the absorption bands at 2162 and 2182 cm^{-1} with integral absorption coefficients of 2.6 cm/μmol [72,80] and 2.2 cm/μmol [53,81], respectively. The number of BAS (OH groups with CO adsorption band at 2162 cm^{-1}) is 2 μmol/g and 8 μmol/g, the number of LAS is 18 and 35 μmol/g for the samples **A** and **D**, respectively. The calculated LAS strength in units of CO adsorption heat [72] is 30 kJ/mol, which is close to that evaluated for Zr-MOFs (27–29 kJ/mol) [53,82] and slightly lower than the one acquired previously for Ti- and Nb-silicates (32 and 36 kJ/mol, respectively) [80]. The number of LAS estimated for Zr-silicates by the IR technique is also close to that found for Ti- and Nb-silicates, thereby indicating similar accessibility to active sites in all the metal-silicates prepared by the same EISA methodology.

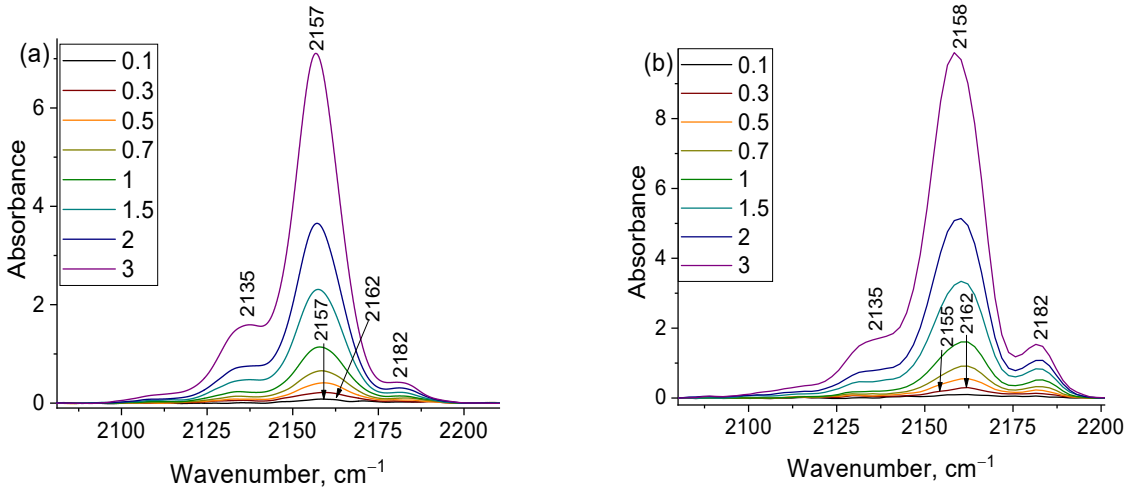

Figure 8. Differential FTIR spectra of CO adsorbed on (**a**) sample **A** and (**b**) sample **D** at −196 °C and a pressure of 0.1–3 Torr.

Basic properties of the samples were studied using FTIR spectroscopy of adsorbed deuterochloroform. Figure 9 shows the FTIR spectra of samples **A** and **D** after adsorption of $CDCl_3$. The spectra show an absorption band in the region of 2200–2300 cm^{-1}, which can be deconvoluted into two individual Gaussian components with maxima at 2262 and 2268 cm^{-1} corresponding to hydrogen-bonded complexes of $CDCl_3$ with the basic sites of the samples and $CDCl_3$ in the gas phase, respectively [53,80,83]. The concentration of the basic sites determined from the integrated intensity of the absorption band at 2262 cm^{-1} is 1403 μmol/g and 1918 μmol/g, for the samples **A** and **D**, respectively. The strength of the basic sites characterized by the proton affinity [53,72,80] is 780 kJ/mol, which corresponds to weak basic sites. This value is similar to the one previously reported for the niobium-silicates prepared by EISA [80] and lower than the values of this parameter evaluated for various Zr-MOFs (840–860 kJ/mol) [53,82] and zirconium oxide (900 kJ/mol) [84]. Most likely, the basic sites are represented by oxygen of the surface ZrOH groups [82].

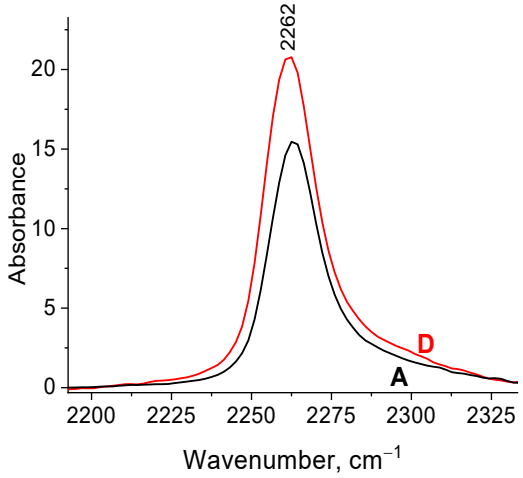

Figure 9. FTIR spectra of deuterochloroform adsorbed on samples **A** and **D**.

2.2. Catalytic Activity of Zr-Silicates in H_2O_2-Based Oxidation of Alkenes

Catalytic performance of Zr-MMM-E (samples **A**–**D**) and Zr/SiO_2 was assessed in the oxidation of three representative alkenes, cyclohexene (CyH), cyclooctene (CyOct), and *trans*-caryophyllene (CP) with 30% aqueous H_2O_2 using acetonitrile as a solvent. The main results are summarized in Tables 2–4.

Cyclohexene was chosen because it serves as a conventional test substrate to evaluate contributions of homo- and heterolytic oxidation pathways by analysis of the composition of the reaction products (Scheme 1) [85]. Regardless of the method of their synthesis, all samples of Zr-MMM-E and Zr/SiO_2 exhibited similar activity (Table 2). With equimolar amount of the oxidant, CyH conversions practically did not exceed the one obtained in a 'blank' experiment with no catalyst (Table 2, entry 1). However, the amount of the two-electron oxidation product epoxide increased in comparison to the amount of one-electron (allylic) oxidation products, cyclohexenyl hydroperoxide (HP), 2-cyclohexene-1-ol (enol), and 2-cyclohexene-1-one (enone) (compare entry 1 with entries 3, 7, 9, 11 and 13).

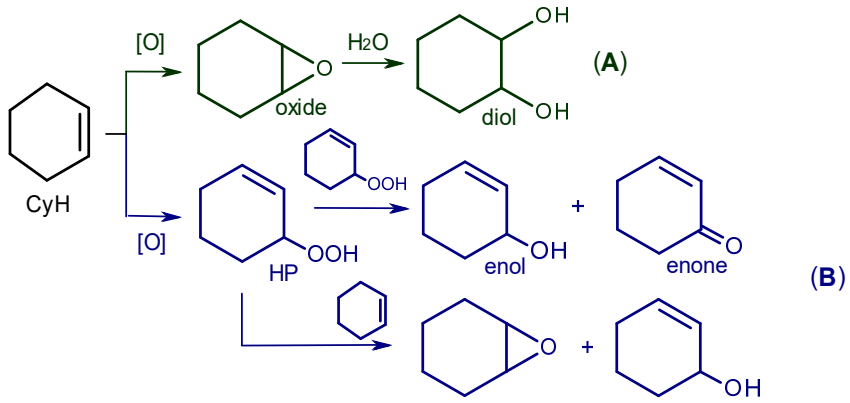

Scheme 1. Cyclohexene oxidation pathways: (**A**) heterolytic (with metal-peroxo species) giving primarily epoxide-relevant products and (**B**) homolytic (radical-mediated) with mostly allylic oxidation products.

Table 2. Cyclohexene oxidation with H_2O_2 in the presence of various Zr-Si catalysts [a].

Entry	Catalyst	Time, [b] h	CyH conv., %	Product Selectivity, [c] %		
				Epoxide	Diol	Allylic [d]
1 [e]	-	1.5	6	16	16	65
2 [f]	H^+	1.5	9	43	21	28
3	**A**	1.5	7	31	15	39
4	**A** + H^+	0.3	27	74	19	4
5 [g]	**A** + H^+	0.3	27	78	15	4
6 [h]	**A** + NaOAc	1	4	25	25	26
7	**B**	3	7	31	15	31
8	**B** + H^+	0.5	23	70	22	6
9	**C**	4	6	33	9	34
10	**C** + H^+	0.3	25	66	28	4
11	**D**	2	8	31	13	26
12	**D** + H^+	0.3	29	73	17	4
13	Zr/SiO_2	1.5	8	25	19	38
14	Zr/SiO_2 + H^+	0.3	21	67	24	5

[a] Reaction conditions: CyH 0.1 mmol, catalyst 10 mg (0.003 mmol Zr), H_2O_2 (30% aq.) 0.1 mmol, $HClO_4$ 0.003 mmol (if added), CH_3CN 1 mL, 50 °C. [b] Optimal reaction time to reach the maximum selectivity and conversion. [c] Based on substrate consumed. [d] Sum of allylic oxidation products (HP + enol + enone). [e] No catalyst was present. [f] 0.003 mmol $HClO_4$. [g] 77% aq. H_2O_2 was used as oxidant. [h] 0.003 mmol of NaOAc was added.

Recently, it has been reported that in situ addition of a source of protons to various Zr-MOF catalysts is a useful tool to increase the oxidation rate and reduce of the yield of allylic oxidation products in the CyH oxidation with H_2O_2 [53,86]. Indeed, the addition of

1 mol equiv (relative to Zr atoms in the silicate) of $HClO_4$ increased significantly the attainable CyH conversion, reduced the reaction time and altered the composition of products, favoring the formation of epoxide along with diol, with total selectivity toward heterolytic oxidation products up to 94 % (Table 2, entries 4, 8, 10, 12 and 14). In the absence of a Zr catalyst, the impact of the acid was much lower (Table 2, entry 2). The use of concentrated H_2O_2 (77%) instead of the dilute one (30%) led to a slight increase in the yield of epoxide with respect to the one of diol (Table 2, entry 5). The addition of 1 mol equiv of NaOAc to a Zr catalyst produced a negative effect on the catalytic activity (Table 2, entry 6).

Therefore, in this case too, acid additives favor the formation of active Zr peroxo species (most likely, hydroperoxo ones [52]). This seems to be a general phenomenon that operates with different types of Zr-catalysts, including Zr-silicates and Zr-MOFs.

Surprisingly, Zr-silicates exhibited rather low activity and selectivity in the epoxidation of cyclooctene (Table 3), the alkene substrate that often features good yields of epoxides with most of the known catalysts [80,87,88]. Higher conversion and epoxide selectivity were attained over sample **D** with a high fraction of oligomeric ZrO_2 species, but, even in this case, a maximum 40% substrate conversion and 50% epoxide selectivity could be achieved using a two-fold excess of the oxidant. It is noteworthy that about 70% of H_2O_2 remained unused. The epoxide selectivity decreased with the reaction time (increased conversion), which is also atypical for CyOct, whose epoxide is generally considered ring-opening resistant. Indeed, independent experiments, in which CyOct epoxide was used as a substrate, showed no significant conversion of this compound under the reaction conditions. These observations suggest that some unidentifiable, probably, polymeric products are accumulated during the reaction course. As in the case of the CyH oxidation, acid additives accelerated CyOct oxidation and led to higher conversions. However, CyOct epoxide yield decreased markedly (see Table 3).

Table 3. Cyclooctene oxidation with H_2O_2 in the presence of Zr-Si catalysts [a].

Catalyst	Time, h	CyOct conv., %	Selectivity to Epoxide, [b] %
A	2	13	31
	5	27	19
A + H$^+$ [c]	2	28	14
D	2	20	50
	5	40	38
Zr/SiO_2	2	18	39
	5	39	28

[a] Reaction conditions: CyOct 0.1 mmol, catalyst 20 mg (0.005 mmol Zr), H_2O_2 (30% aq.) 0.2 mmol, CH_3CN 1 mL, 50 °C. [b] Based on substrate consumed. [c] $HClO_4$ 0.005 mmol.

On the contrary, the oxidation of caryophyllene, a bulky natural terpene, with 2 equiv of H_2O_2 in the presence of Zr-MMM-E catalysts (samples **A** and **D)** as well as Zr/SiO_2 produced endocyclic monoepoxide (Scheme 2) with fairly good substrate conversions and product yields (Table 4). Note that CP epoxide is a valuable product approved by FDA as a food and cosmetic stabilizer [89] and used as a flavoring substance with the scent of cloves too [90]. In contrast with CyH and CyOct oxidation, epoxidation of CP easily proceeds without acid additives too. As in the case of CyOct oxidation, sample **D** displayed the highest activity among the catalysts studied. Conversion of CP attained 87% after 5 h, whereas it reached only 69% over sample **A**. The selectivity to monoepoxide for all Zr-silicates reached 78–80%. It is noteworthy that CP was practically the only alkene substrate that revealed good epoxide yields in H_2O_2-based oxidations over Zr-MOFs [53]. Interestingly, other electron-rich alkenes, e.g., 3-carene and limonene, as well as tetramethylethylene gave significantly lower conversions and epoxide yields, indicating that

nucleophilicity of the C=C double bond is not the main factor affecting the epoxidation efficiency. For instance, Zr/SiO_2 was able to convert limonene into 1,2-limonene epoxide with an epoxide yield of 23% in 1 h [91], whereas Nb/SiO_2, obtained via OM-DI from niobocene dichloride, was able to attain an epoxide yield of 46% in 1 h under the same conditions [30]. Therefore, we may suggest that some other factors, in particular alkene (epoxide) bulkiness, has a strong impact on the epoxidation over Zr-catalysts.

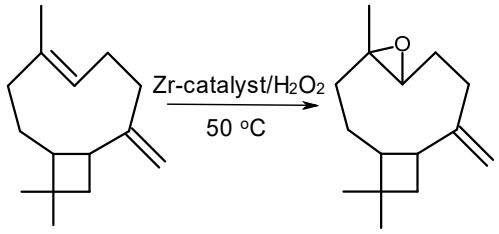

Scheme 2. Oxidation of *trans*-caryophyllene with H_2O_2 over Zr-silicates.

Table 4. Caryophyllene oxidation with H_2O_2 in the presence of Zr-Si catalysts [a].

Catalyst	Time, h	CP conv, %	Selectivity to Epoxide, [b] %
A	2	40	78
	5	69	78
D	2	63	76
	5	87	77
D [c,d]	2	45	75
	5	64	70
Zr/SiO_2	2	37	78
	5	65	80
UiO-67 [e]	4	44	92

[a] Reaction conditions: CP 0.1 mmol, catalyst 20 mg (0.005 mmol Zr), H_2O_2 (30% aq.) 0.2 mmol, CH_3CN 1 mL, 50 °C. [b] Yield of endocyclic monoepoxide based on substrate consumed. [c] H_2O_2 0.1 mmol. [d] H_2O_2 efficiency 90%. [e] catalyst 2 mg (0.007 mmol Zr), H_2O_2 0.1 mmol, CH_3CN 1 mL, 50 °C (data taken from ref. [53]).

Figure 10 shows comparison of the catalytic performance of Zr-MMM-E in CP oxidation with that of Ti- and Nb-silicates prepared by the same EISA methodology. While the highest activity was observed over Nb-MMM-E, Zr-MMM-E proved to be more active than Ti-MMM-E. Selectivity to CP epoxide attained 77%, 80% and 74% for Zr-, Nb- and Ti-MMM-E, respectively.

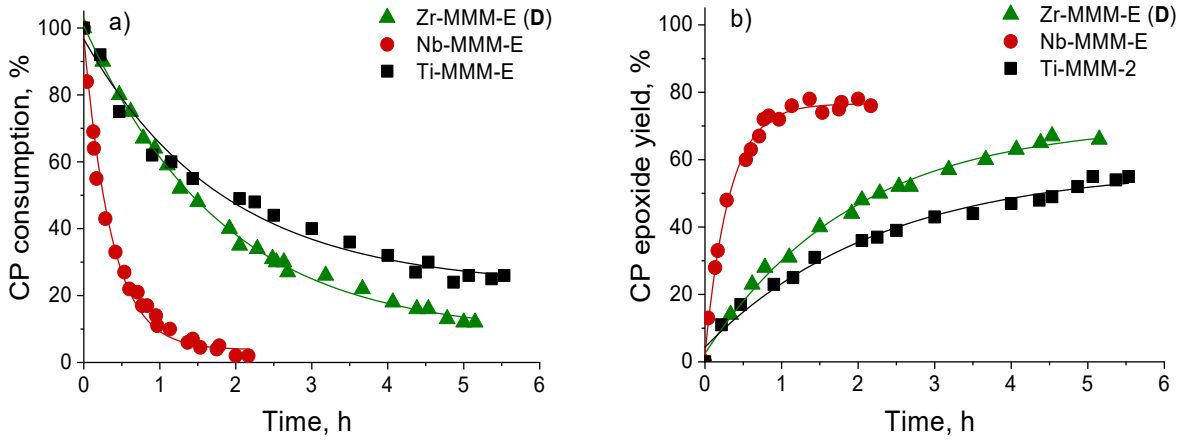

Figure 10. Comparison of catalytic performances of Zr-MMM-E, Nb-MMM-E and Ti-MMM-E in CP epoxidation with H_2O_2: kinetic curves for (**a**) CP consumption and (**b**) CP epoxide yield. Reaction conditions: CP 0.1 mmol, H_2O_2 0.2 mmol, catalyst (0.005 mmol Zr, Nb or Ti), CH_3CN 1 mL, 50 °C.

2.3. Catalytic Activity of Zr-silicates in H_2O_2-Based Oxidation of Methyl Phenyl Sulfide

The oxidation of a representative thioether, methyl phenyl sulfide, over Zr-Si catalysts was investigated as well. In this reaction, the primary oxidation product is sulfoxide (MPSO) that is oxidized further to produce sulfone ($MPSO_2$) (Scheme 3).

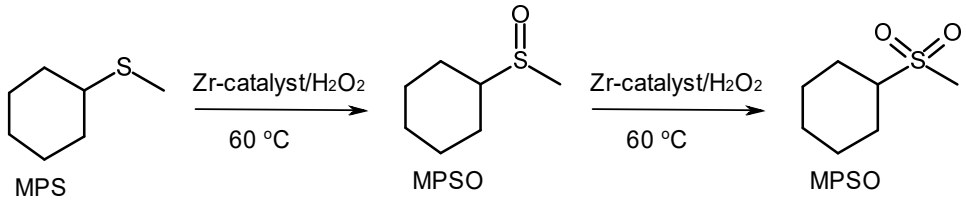

Scheme 3. Oxidation of methyl phenyl sulfide with H_2O_2 over Zr-silicates.

The product distribution in thioether oxidation with equimolar amount of oxidant allows one to suggest the nature of the oxidizing species, electrophilic or nucleophilic. While sulfoxides are products of electrophilic oxidation of sulfides, which are strong nucleophiles, sulfones can be produced via both electrophilic and nucleophilic oxidation of sulfoxides, which possess a biphilic nature [92]. Earlier, we have found that H_2O_2-based oxidation of MPS and other thioethers in the presence of Zr-MOFs, in particular UiO-66, occurs via predominantly nucleophilic mechanism, leading to the formation of sulfone with selectivity up to 99% at ca. 50% MPS conversion [53,82].

The main results on the MPS oxidation with 1 equiv of H_2O_2 over Zr-Si catalysts are presented in Table 5. For all Zr-MMM-E samples and the OM-DI-derived catalyst Zr/SiO_2, sulfone was the prevailing product formed with selectivity 62–74% at 51–57% MPS conversion. Catalyst **A,** having mostly 'isolated' zirconium centers, was less active and gave more sulfone than the other catalysts that possess oligomeric ZrO_2 species. Again, sample **D** was the most active one among the series of Zr-MMM-E catalysts. The Zr/SiO_2 sample showed a higher initial oxidation rate than all Zr-MMM-E solids, but MPS conversion and products yields were similar to the ones obtained with samples **B**, **C** and **D** (Table 5). The oxidant utilization efficiency values were as high as 89–93% for Zr-MMM-E samples and 86% for the Zr/SiO_2 catalyst.

Table 5. Methyl phenyl sulfide oxidation with H_2O_2 in the presence of Zr-Si catalysts [a].

Catalyst	Time, [b] h	MPS conv, %	Product Selectivity, [c] %		H_2O_2 Efficiency, [d] %
			MPSO	$MPSO_2$	
A	2	51	26	74	89
B	1.5	55	36	64	90
C	1.5	55	36	64	90
D	1	57	37	63	93
Zr/SiO_2	0.5	53	38	62	86

[a] Reaction conditions: MPS 0.1 mmol, catalyst 5 mg (0.0013 mmol Zr), H_2O_2 (30% aq.) 0.1 mmol, CH_3CN 1 mL, 60 °C. [b] Optimal reaction time to reach the maximum selectivity and conversion. [c] Based on substrate consumed. [d] H_2O_2 utilization efficiency = total yield of products based on the oxidant consumed.

2.4. Mechanism of Alkene and Thioether Oxidation with H_2O_2 over Zr-Silicate Catalysts

The prevalent formation of sulfone over sulfoxide in the MPS oxidation with one equivalent of the oxidant clearly indicates predomination of nucleophilic oxidizing species over electrophilic ones in the presence of Zr-catalyst and H_2O_2 [82] and references cited therein. Given that di(oligo)nuclear species certainly prevail in the most active Zr-silicate catalysts, we may suggest a hydrogen peroxide activation mechanism similar to the one we proposed earlier for Zr-MOFs (Scheme 4). In this mechanism, the first step is the formation of an electrophilic Zr hydroperoxo species 'ZrOOH', which is responsible for the oxygen transfer to a C=C bond in the alkene and nucleophilic S atom in the thioether. The presence of weak basic sites (most probably ZrOH) favors the transformation of 'ZrOOH' to a nucleophilic peroxo Zr species, 'ZrOO$^-$', which acts as the oxidant toward the sulfoxide bound to the neighboring Zr site.

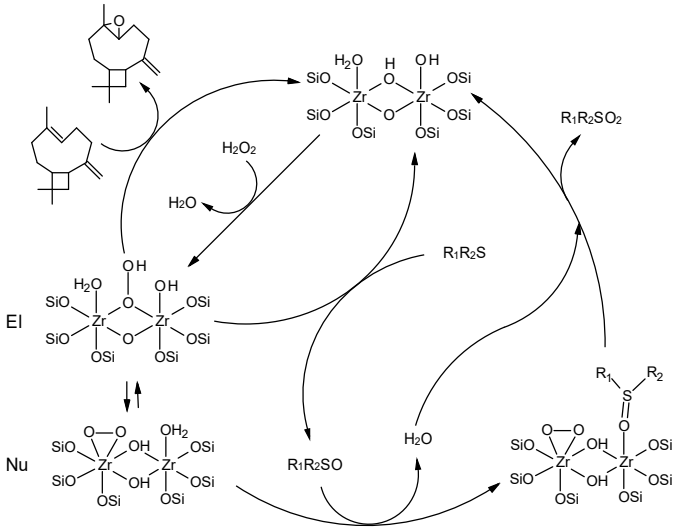

Scheme 4. Tentative mechanism of CP and MPS oxidation with H_2O_2 over Zr-silicate.

2.5. The reasons for Zr-Si Catalyst Deactivation

Zr-silicate-catalyzed epoxidation is typically characterized by relatively low alkene conversion values. Thus, with 1 equiv of oxidant, the maximal CyH conversion attained 23–29%, without a significant alteration in the product selectivity (Table 2). The incomplete substrate conversion might be caused by competitive decomposition of H_2O_2 with evolution of molecular oxygen. However, we have found that the rate of unproductive H_2O_2 decomposition over Zr-MMM-E was rather low in comparison with Nb- and Ti-silicates (Figure 11a), for which significantly higher CyH conversions could be achieved [32] (Figure 11b). Indeed, H_2O_2 utilization efficiency in the presence of Zr-MMM-E (sample **A**)

and 1 equiv of H^+ attained 90%, indicating that the reaction stopped before all H_2O_2 was consumed. Therefore, unproductive degradation of the oxidant cannot be the main reason for low alkene conversions in the presence of Zr-silicates.

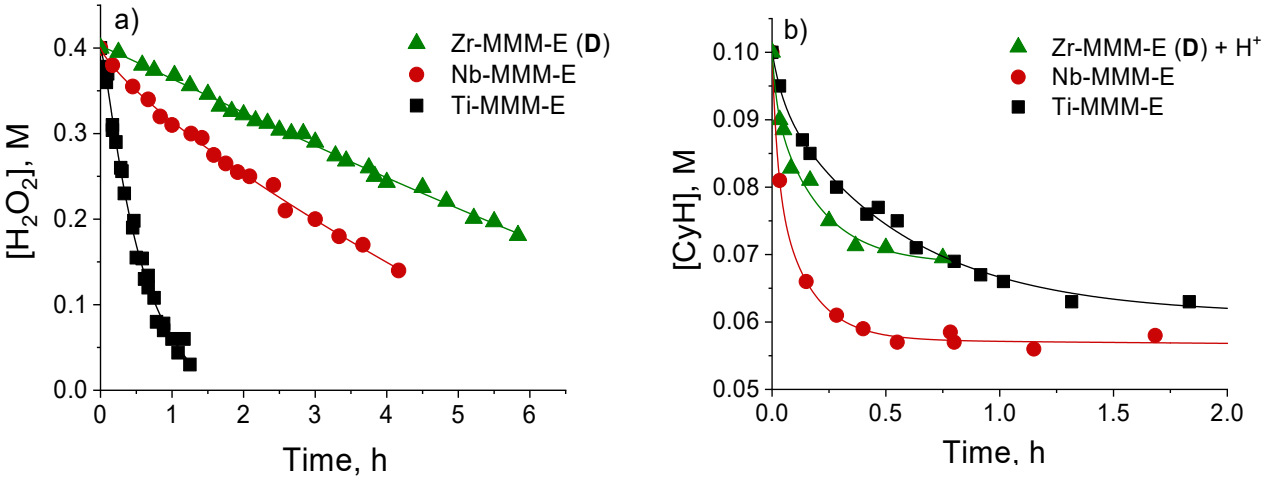

Figure 11. Comparison of catalytic activity of Zr-MMM-E, Nb-MMM-E and Ti-MMM-E in (**a**) H_2O_2 decomposition (reaction conditions: H_2O_2 0.4 M, catalyst 0.016 mmol of Zr, Nb or Ti, 70 °C, CH_3CN 5 mL) and (**b**) CyH oxidation (reaction conditions as in Table 2, catalyst 0.003 mmol of Zr, Nb or Ti).

Another reason for fast catalyst deactivation could be the accumulation of the reaction products inside the pores and/or their strong binding to zirconium active sites. However, physical adsorption of the product could hardly be the reason for catalyst deactivation, otherwise the same phenomenon would be observed for Nb- and Ti-catalysts as well, which is not the fact. This means that a specific chemical binding of products to oxophilic Zr(IV) sites can play a critical role. Previously, we have shown that oxidation products (epoxide/diol and water) caused the catalyst deactivation in the CyH oxidation over UiO-66 [86]. Interestingly, in the case of Zr-MMM-E, only epoxide additives dramatically slowed down the CyH oxidation process, without reaching the expected substrate conversion, while the addition of CyH diol or H_2O into the reaction mixture produced no effect at all (Figure 12).

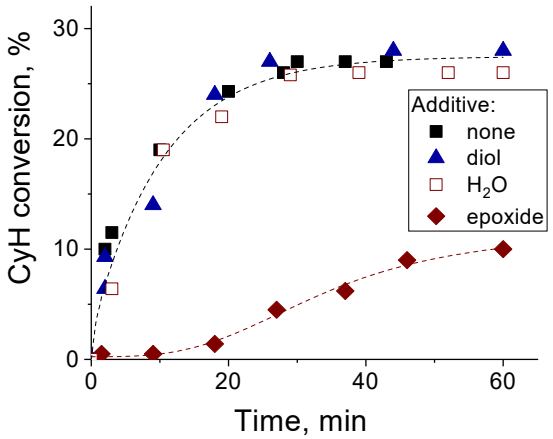

Figure 12. Effect of reaction products on CyH oxidation with H_2O_2 over Zr-MMM-E (sample **A**) and 1 equiv of $HClO_4$. Reaction conditions: CyH 0.1 mmol, catalyst 10 mg (0.003 mmol Zr), H_2O_2 (30% aq.) 0.1 mmol, $HClO_4$ 0.003 mmol, CH_3CN 1 mL, 50 °C. Additives: 0.02 mmol of CyH-epoxide or 0.015 mmol of CyH-diol or 0.3 mmol of H_2O (added in the beginning of the reaction).

In sharp contrast, the addition of CP epoxide produced no rate-retarding effect on the oxidation of CP itself (Figure 13). Given that CP epoxide is a large molecule, we may assume that, because of its bulkiness, it likely prevents the coordination of the epoxide oxygen atom to Zr(IV) sites. This specific feature enables high epoxidation yields in CP oxidation over Zr-catalysts.

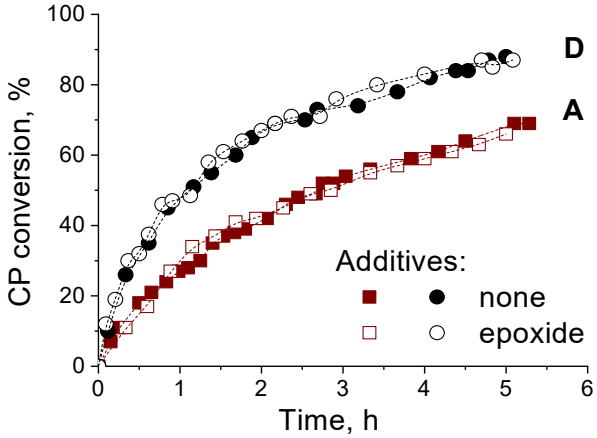

Figure 13. Effect of reaction products on CP oxidation with H_2O_2 over Zr-MMM-E (samples **A** and **D**). Reaction conditions: CP 0.1 mmol, catalyst 20 mg (0.005 mmol Zr), H_2O_2 (30% aq.) 0.2 mmol, CH_3CN 1 mL, 50 °C. Additive: 0.02 mmol of CP epoxide (added in the beginning of the reaction).

Specific adsorption study (see Section 3.5 for details) revealed some adsorption of sulfoxide (about 10% from a 0.1 M solution in CH_3CN) and no adsorption of sulfide and sulfone on Zr-MMM-E (sample **D**). However, the addition of sulfoxide to the reaction mixture produced minor effect on the MPS oxidation over Zr-MMM-E (Figure 14), which is due to fast oxidation of sulfoxide to sulfone.

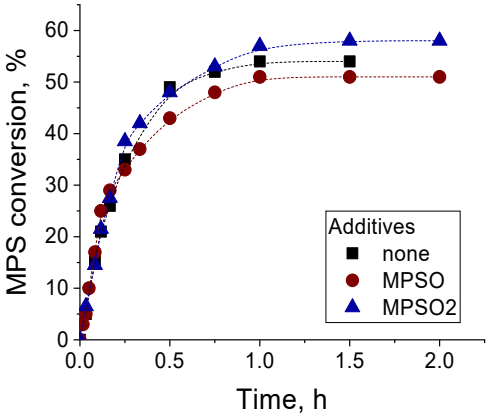

Figure 14. Effect of reaction products on MPS oxidation with H_2O_2 over Zr-MMM-E (sample **D)**. Reaction conditions: MPS 0.1 mmol, catalyst 5 mg (0.0013 mmol Zr), H_2O_2 (30% aq.) 0.1 mmol, CH_3CN 1 mL, 60 °C. Additives: 0.02 mmol of MPSO or $MPSO_2$ (added in the beginning of the reaction).

2.6. Catalyst Stability and Reusability

The stability of the structure of Zr-Si catalysts in the presence of aqueous H_2O_2 was checked by means of XRD technique. XRD patterns of both sample **A** and sample **D** remained intact after treatment with an aqueous-acetonitrile solution of H_2O_2 (Figure 15).

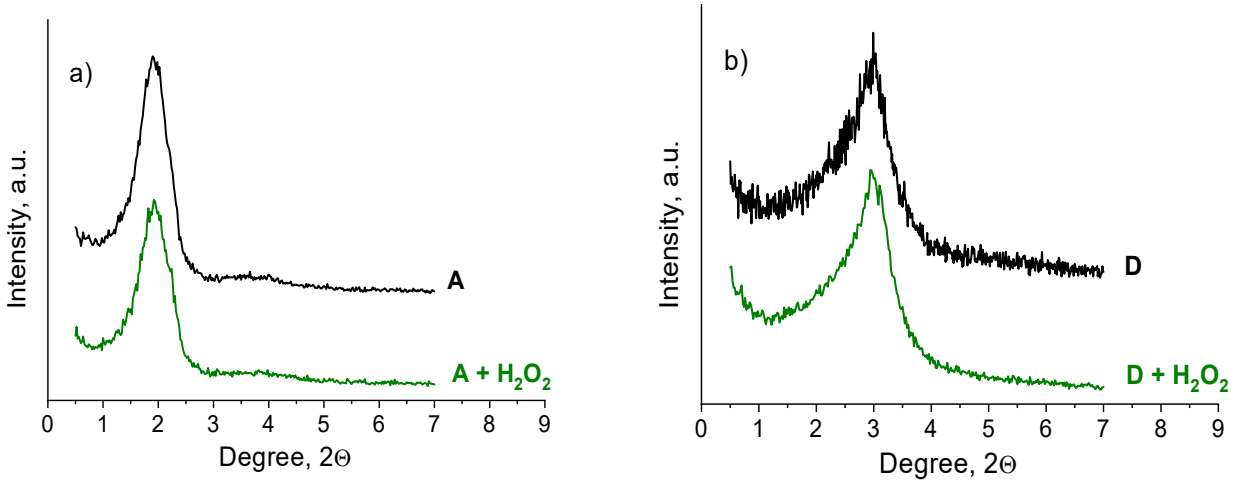

Figure 15. XRD patterns of samples (**a**) **A** and (**b**) **D**: initial and after treatment with H_2O_2 in MeCN.

The nature of the catalysis over Zr-MMM-E was verified for both alkene and MPS oxidation by hot filtration tests. Practically no further substrate conversion was observed after removal of the catalyst, indicating the truly heterogeneous nature of the observed catalysis (Figure 16). The solid and filtrate were also studied by elemental analysis using ICP-AES. It was found that Zr content in the sample remains intact while the amount of Zr in the filtrates is below 1 ppm, which confirms the absence of metal leaching under the conditions employed.

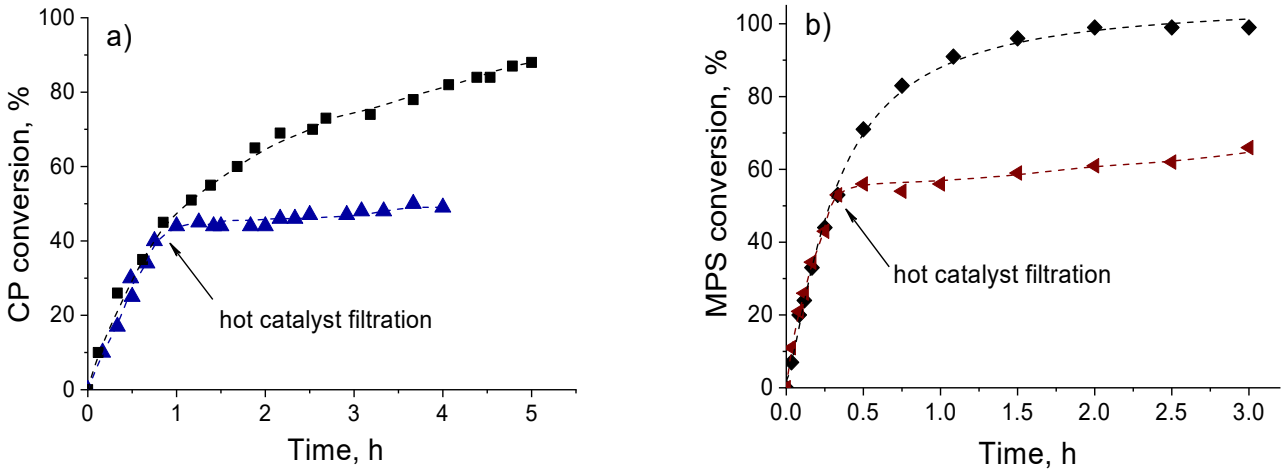

Figure 16. Hot catalyst filtration test for (**a**) CP and (**b**) MPS oxidation with H_2O_2 in the presence of Zr-MMM-E (sample **D**). Reaction conditions: MPS 0.1 mmol, catalyst 5 mg (0.0013 mmol Zr), H_2O_2 (30% aq.) 0.22 mmol, CH_3CN 1 mL, 60 °C.

The recycling behavior of the most active catalysts, sample **D**, was studied in several consecutive runs in the oxidation of CP and MPS with 30% H_2O_2 (Figure 17a,b), respectively). The catalyst was regenerated by calcination at 550 °C between the runs. The catalyst revealed a rather stable recycling performance in the CP epoxidation (Figure 17a) and MPS oxidation (Figure 17b). Although some reduction of the turnover frequency (TOF) could be observed after the first use in MPS oxidation, the TOF remained constant and even increased during the subsequent runs.

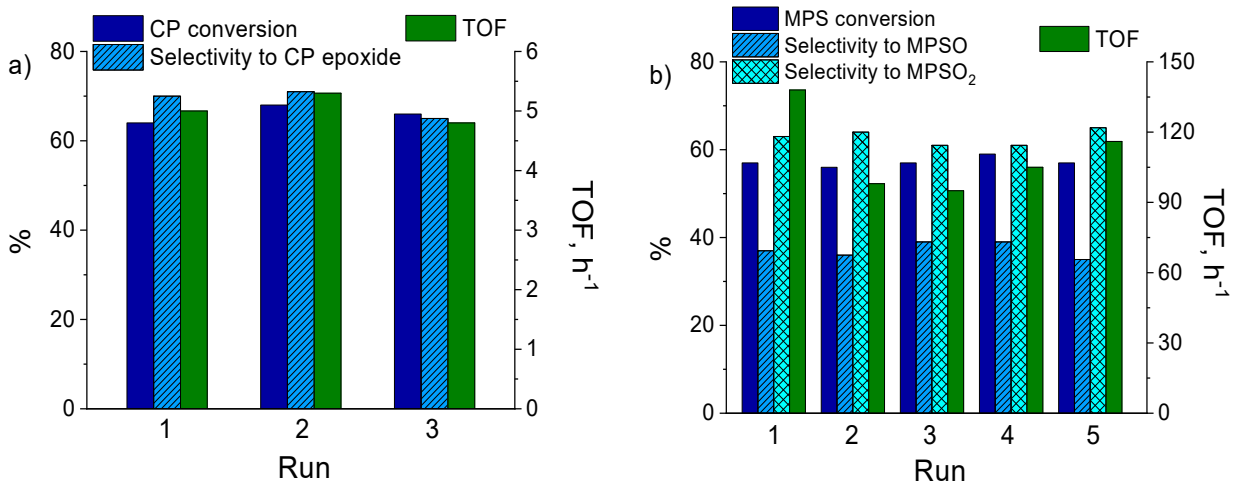

Figure 17. Reuse of sample **D** in (**a**) CP and (**b**) MPS oxidation with H_2O_2. Reaction conditions: (**a**) CP 0.1 mmol, H_2O_2 (30% aq.) 0.1 mmol, catalyst 20 mg (0.005 mmol Zr), CH_3CN 1 mL, 50 °C; (**b**) MPS 0.1 mmol, H_2O_2 (30% aq.) 0.1 mmol, catalyst 5 mg (0.0013 mmol Zr), CH_3CN 1 mL, 60 °C. TOF = (moles of substrate consumed)/(moles of Zr × time).

3. Materials and Methods

3.1. Materials

Cetyltrimethylammonium bromide (CTAB, 99+%), tetraethyl orthosilicate (TEOS, 98+%), zirconium(IV) acetylacetonate ($Zr(C_5H_7O_2)_4$) (97%), 98.5% (-)-*trans*-caryophyllene, were purchased from Sigma-Aldrich. Methyl phenyl sulfide (99%) was purchased from Acros. CyH and CyOct were purchased from Sigma-Aldrich and purified prior to use by passing through a column filled with neutral alumina to remove traces of possible oxidation products. Acetonitrile (HPLC–grade, Panreac) was dried and stored over activated 4 Å molecular sieves. Ethanol (95 %), ethylacetate and other reactants were obtained commercially and used without any additional purification. The concentration of H_2O_2 (30 or 77 wt.% in water) was determined iodometrically prior to use. Deionized water (EASY pure, RF, Barnsted) was used for the preparation of catalysts.

3.2. Catalyst Preparation and Characterization

Preparation of $Zr(acac)_4$ solution. A typical procedure was as follows: 0.44 g (0.9 mmol) $Zr(acac)_4$ were dissolved in 8 mL of ethanol (95%) and mixed for 1 h at room temperature with periodical heating at 40 °C until complete dissolution.

Synthesis of Zr-MMM-E by EISA. In a standard procedure, surfactant, CTAB (2.75 g, 7.5 mmol) was dissolved in ethanol (95%, 73 mL) under vigorous stirring for 2 h at room temperature. Then TEOS (11.2 mL, 0.05 mol), deionized H_2O (6 mL), 36.5% HCl (6 μL, 0.07 mmol) and the solution of the $Zr(acac)_4$ in ethanol (see above) were added under vigorous stirring. The reaction mixture was stirred (750 rpm) for 30 s and then the resulting clear sol was left in an open Petri dish under ambient conditions until full evaporation of the solvent. The as–made solid was calcined at 550 °C for 5 h in the air with a temperature ramp of 1 °C/min to remove the organic species. The solid was designated as sample **A**. For the preparation of samples **B**, **C** and **D**, the amount of HCl was increased to 77 (0.9 mmol, 1 equiv to Zr), 154 (1.8 mmol, 2 equiv to Zr), and 532 μL (6.3 mmol, 7 equiv to Zr), respectively.

Synthesis of Ti-MMM-E and Nb-MMM-E by EISA. For comparison, mesoporous titanium and niobium silicates with oligomeric Ti(IV) and Nb(V) sites were prepared by the same EISA approach following the protocols reported earlier [27] and [32], respectively. Textural properties for Ti-MMM-E (Ti 2.5 wt.%): S_{BET} = 1040 m^2/g, V_p = 0.68 cm^3/g, D_p = 2.6 nm; for Nb-MMM-E (Nb 1.85 wt.%): S_{BET} = 1138 m^2/g, V_p = 0.59 cm^3/g, D_p = 2.9 nm.

Synthesis of Zr/SiO₂. The Zr/SiO_2 catalyst was obtained via solventless organometallic precursor dry impregnation of commercial SiO_2 (Grace Davison, LC60A; S BET 529 m^2/g, pore volume 0.88 cm^3/g, mean pore diameter 2.0–8.0 nm (very broad distribution with a maximum at 5.4 nm). The silica support was rehydrated with high purity deionized (18 MΩ cm) water (MilliQ Academic, Millipore) for 2 h and then dried at the rotary evaporator. The sample was calcined at 300 °C for 1 h in air and overnight under dynamic vacuum. *Bis*(cyclopentadienyl)zirconium(IV) dichloride (98% Sigma-Aldrich) was finely milled and added under inert atmosphere in solid phase to the silica. The solid mixture was stirred overnight under static vacuum at 150 °C. The mixture was calcined under oxygen at 500 °C for 2 h to obtain the final catalyst.

The freshly calcined samples were characterized by elemental analysis, N_2 adsorption, X–ray diffraction, TEM, Raman, and diffusion reflectance UV−vis techniques and used for catalytic tests.

3.3. Catalytic Oxidations

Catalytic reactions were performed under vigorous stirring (500 rpm) in thermostated glass vessels. Typical reaction conditions for CyH oxidation were as follows: CyH 0.1 M, H_2O_2 0.1 M, Zr-Si catalyst 10 mg (0.003 mmol Zr), CH_3CN, 1 mL, 50 °C, 2 h. Typical reaction conditions for CyOct and CP oxidations were as follows: CyOct or CP 0.1 M, H_2O_2 0,1–0.2 M, Zr-Si catalysts 20 mg (0.005 mmol Zr), CH_3CN, 1 mL, 50 °C, 2–5 h. Typical reaction conditions for MPS oxidation: MPS 0.1 M, H_2O_2 0.1 M, Zr-MMM-E 5 mg (0.0014 mmol Zr), CH_3CN, 1 mL, 60 °C, 0.5–2 h. Reactions were started by the addition of H_2O_2 to the reaction mixture. Samples of the reaction mixture were withdrawn periodically during the reaction course by a syringe through a septum. Each experiment was reproduced 2–4 times. The oxidation products were identified by the comparison of gas chromatography (GC) retention time with the retention time of the authentic samples. Product yields and substrate conversions were quantified by GC using biphenyl as an internal standard.

3.4. Hydrogen Peroxide Decomposition

Decomposition of H_2O_2 (0.4 M) was studied in the absence of organic substrate at 70 °C in CH_3CN (5 mL) in the presence of M-MMM-E catalysts (M = Ti, Nb or Zr, 0.016 mmol). Aliquots of 0.2 mL were taken during the reaction course, and H_2O_2 concentration was determined by iodometric titration. Each experiment was reproduced 2–3 times.

3.5. Sorption Studies

MPS, MPSO and MPSO sorption studies were performed in thermostated glass vessels under vigorous stirring (500 rpm). 1 mL of 0.1 M solution of MPS, MPSO or $MPSO_2$ in CH_3CN were added to 10 mg of Zr-MMM-E (sample **A**) and stirred during 1 h at 27 °C. The aliquots were taken from solution by syringe and analyzed by GC using biphenyl as an internal standard to quantify the concentration.

3.6. Hydrothermal Stability and Stability towards Aqueous H_2O_2

To estimate the stability toward aqueous H_2O_2, samples **A** and **D** was treated with aqueous 30% H_2O_2 for 1 h (100 mg of catalyst, 0.11 M H_2O_2, 20 mL MeCN, 25 °C), dried in air and calcined at 550 °C before physicochemical measurements.

3.7. Instrumentation

GC analyses were performed using a gas chromatograph Tsvet–500 or Chromos GH-1000 equipped with a flame ionization detector and a quartz capillary column (30 m×0.25 mm) filled with Agilent DB–5MS.

XRD measurements were performed on a high precision X–ray diffractometer mounted on beamline No.2 of the VEPP–3 storage ring at Siberian Synchrotron Radiation Center (SSRC). The radiation wavelength was 0.15393 nm. A high natural collimation of

the synchrotron radiation beam, a flat perfect crystal analyzer, and a parallel Soller slit on the diffracted beam limiting its azimuthal divergence provided an extremely high instrumental resolution in a small angle region of $2\theta = 0.5 \div 10°$ and higher.

Nitrogen adsorption measurements were carried out at 77 K using a NOVA 1200 instrument (Quantachrome) within the partial pressure range 10−4–1.0. The catalysts were degassed at 150 °C for 24 h before the measurements. Surface areas of the Zr–MMM–E samples were determined by the BET analysis of low–temperature N_2 adsorption data. Pore size distributions were calculated from the adsorption branches of the nitrogen isotherms by means of the regularization procedure, using reference local isotherms calculated in a cylindrical silica pore model in the framework of the density functional theory (DFT) approach. Special software provided by Quantachrome Corp. was used for this purpose. Mean pore diameters were calculated as mathematical expectation values from these distributions.

Zirconium content in the solids and in the filtrate, which remained after separation of the catalysts from the reaction mixture, was determined by ICP–OES using a Perkin-Elmer Optima-430 DV instrument.

The state of zirconium in the catalysts was studied by DR UV–vis spectroscopy under ambient conditions using a Shimadzu UV–VIS 2501PC spectrophotometer. FT–Raman spectra (3600–100 cm^{-1}, 300 scans, resolution 4 cm^{-1}, 180° geometry) were recorded using a RFS 100/S spectrometer (Bruker). Excitation of the 1064 nm line was provided by an Nd–YAG laser (100 mW power output). Infrared spectra of adsorbed CO and $CDCl_3$ were recorded on a Shimadzu IRTracer-100 spectrometer in the range of 400–6000 cm^{-1} with a resolution of 4 cm^{-1} and acquisition of 200 scans. Before adsorption of probe molecules, the samples pressed into thin pellets (20–25 mg/cm^2) were evacuated in an IR cell at 500 °C for 1h. CO adsorption was performed at −196 °C and CO pressure from 0.1 to 10 Torr. $CDCl_3$ was adsorbed at 20 °C. Transmission electron microscopy (TEM) data were obtained using a Thermo Fisher Scientific Themis Z (Netherlands) electron microscope operated at 200 kV. Images with a high atomic number contrast were acquired using a high angle annular dark field (HAADF) detector in scanning-TEM (STEM) mode. The local composition of the samples was studied using EDX spectroscopy. The samples for the TEM study were prepared on a perforated carbon film mounted on a copper grid.

4. Conclusions

In this work, we demonstrated that mesoporous zirconium-silicates with fairly good dispersion and accessibility of active Zr(IV) sites can be prepared by two different methodologies, evaporation-induced self-assembly and solventless organometallic precursor dry impregnation of commercial SiO_2. These two kinds of materials revealed similar catalytic performances in alkene and thioether oxidation with aqueous H_2O_2 that differed significantly from the catalytic behavior of Ti- and Nb-silicates prepared by the same methodologies, indicating that the nature of the transition metal plays a critical role in the oxidation scenario. In contrast to Ti- and Nb-catalysts, Zr-ones are highly prone to fast deactivation caused by strong adsorption of the epoxide product on Zr sites. However, high epoxide yields can be achieved if bulky electron-rich alkenes, e.g., caryophyllene, are used as substrates. In the thioether oxidation, sulfone predominates over sulfoxide, indicating a nucleophilic oxidation mechanism. These features are also typical of other types of Zr-catalysts, e.g., Zr-MOFs. Therefore, we may suggest that Zr-containing materials deserve a further investigation as heterogeneous catalysts to be potentially applied in the selective oxidation of bulky organic molecules for the production of high added-value products.

Author Contributions: conceptualization, I.D.I., O.V.Z. and O.A.K.; formal analysis, I.D.I., O.V.Z., N.V.M., O.A.S., T.S.G., Y.A.C., A.N.S. and M.G.; investigation, I.D.I., O.V.Z., N.V.M., O.A.S., T.S.G., Y.A.C., A.N.S. and M.G.; methodology, I.D.I., O.V.Z., N.V.M., O.A.S., T.S.G., Y.A.C., A.N.S., M.G. and O.A.K.; visualization, I.D.I., O.V.Z., N.V.M., O.A.S. and T.S.G.; writing—original draft, O.V.Z.;

writing—review & editing, I.D.I., O.V.Z., N.V.M., O.A.S., T.S.G., M.G. and O.A.K.; funding acquisition, N.V.M. and O.A.K.; project administration, O.A.K.; supervision, O.A.K. All authors have read and agreed to the published version of the manuscript.

Funding: This research was partially funded by the Ministry of Science and Higher Education of the Russian Federation within the governmental order for the Boreskov Institute of Catalysis (project AAAA-A21-121011390008-4) and the Russian Foundation for Basic Research (grant 21-53-15010).

Data Availability Statement: Not applicable.

Acknowledgments: The authors thank A.A. Leonova for the N_2 adsorption measurements.

Conflicts of Interest: The authors declare no conflict of interest.

References

1. Sienel, G.; Rieth, R.; Rowbottom, K.T. Epoxides. In *Ullmann's Encyclopedia of Industrial Chemistry*; Wiley-VCH Verlag GmbH & Co. KGaA: Weinheim, Germany, 2000. https://doi.org/10.1002/14356007.a09_531.
2. Clerici, M.G., Kholdeeva, O.A. (Eds.). *Liquid Phase Oxidation* via *Heterogeneous Catalysis: Organic Synthesis and Industrial Applications*; John Wiley & Sons: Hoboken, NJ, USA, 2013; 546p. https://doi.org/10.1002/9781118356760.
3. Duprez, D., Cavani, F. (Eds.). *Handbook of Advanced Methods and Processes in Oxidation Catalysis*; Imperial College Press: London, UK, 2014; 1036p. https://doi.org/10.1142/p791.
4. Sheldon, R.A.; van Bekkum, H. *Fine Chemicals through Heterogeneous Catalysis*; Wiley: Weinheim, Germany, 2001; pp. 473–551. https://doi.org/10.1002/9783527612963.ch09.
5. Mizuno, N. (Ed.). *Modern Heterogeneous Oxidation Catalysis: Design, Reactions and Characterization*; Wiley-VCH: Weinheim, Germany, 2009; 356p. https://doi.org/10.1002/9783527627547.
6. Sheldon, R.A. E factors, green chemistry and catalysis: An odyssey. *Chem. Comm.* **2008**, *10*, 3352–3365. https://doi.org/10.1039/B803584A.
7. Clerici, M.G.; Bellussi, G.; Romano, U. Synthesis of propylene oxide from propylene and hydrogen peroxide catalyzed by titanium silicalite. *J. Catal.* **1991**, *129*, 159–167. https://doi.org/10.1016/0021-9517(91)90019-Z.
8. Forlin, A.; Bergamo, M.; Lindner, J. Production of Propylene Oxide. In *Liquid Phase Oxidation via Heterogeneous Catalysis: Organic Synthesis and Industrial Applications*; Clerici, M.G., Kholdeeva, O.A., Eds.; John Wiley & Sons: Hoboken, NJ, USA, 2013; Chapter 10.3, pp. 474–495, ISBN: 978-0-470-94552-3. https://doi.org/10.1002/9781118356760.ch10.
9. Tanev, P.T.; Chibwe, M.; Pinnavaia, T. Titanium-Containing Mesoporous Molecular Sieves for Catalytic Oxidation of Aromatic Compounds. *Nature* **1994**, *368*, 321–323. https://doi.org/10.1038/368321a0.
10. Sayari, A. Catalysis by Crystalline Mesoporous Molecular Sieves. *Chem. Mater*. **1996**, *8*, 1840–1852. https://doi.org/10.1021/cm950585+.
11. Corma, A. From microporous to mesoporous molecular sieve materials and their use in catalysis. *Chem. Rev*. **1997**, *97*, 2373–2420. https://doi.org/10.1021/cr960406n.
12. Tuel, A. Modification of mesoporous silicas by incorporation of heteroelements in the framework. *Micropor. Mesopor. Mater.* **1999**, *27*, 151–169. https://doi.org/10.1016/S1387-1811(98)00250-9.
13. Kholdeeva, O.A. Selective Oxidations Catalyzed by Mesoporous Metal-Silicates. In *Liquid Phase Oxidation via Heterogeneous Catalysis: Organic Synthesis and Industrial Applications;* Clerici, M.G., Kholdeeva, O.A., Eds.; John Wiley & Sons: Hoboken, NJ, USA, 2013; Chapter 4, pp. 127–219. https://doi.org/10.1002/9781118356760.ch4.
14. Kholdeeva, O.A. Recent Developments in Liquid-Phase Selective Oxidation Using Environmentally Benign Oxidants and Mesoporous Metal-Silicates. *Catal. Sci. Technol*. **2014**, *4*, 1869–1889. https://doi.org/10.1039/C4CY00087K.
15. Dal Santo, V.; Guidotti, M.; Psaro, R.; Marchese, L.; Carniato, F.; Bisio, C. Rational Design of Single-Site Heterogeneous Catalysts: towards High Chemo-, Regio-and Stereoselectivity. *Proceed. Royal Soc. A* **2012**, *468*, 1904–1926. https://doi.org/10.1098/rspa.2012.0056.
16. Cui, X.; Li, W.; Ryabchuk, P.; Junge, K.; Beller, M. Bridging homogeneous and heterogeneous catalysis by heterogeneous single-metal-site catalysts. *Nat. Catal*. **2018**, *1*, 385–397. https://doi.org/10.1038/s41929-018-0090-9.
17. Liang, J.; Liang, Z.; Zou, R.; Zhao, Y. Heterogeneous Catalysis in Zeolites, Mesoporous Silica, and Metal–Organic Frameworks. *Adv. Mater*. **2017**, *29*, 1701139. https://doi.org/10.1002/adma.201701139.
18. Samantaray, M.K.; Pump, E.; Bendjeriou-Sedjerari, A.; D'Elia, A.; Pelletier, J.D.A.; Guidotti, M.; Psaro, R.; Basset, J.M. Surface organometallic chemistry in heterogeneous catalysis, *Chem. Soc. Rev*. **2018**, *47*, 8403–8437. https://doi.org/10.1039/c8cs00356d.
19. Kholdeeva, O.A.; Melgunov, M.S.; Shmakov, A.N.; Trukhan, N.N.; Kriventsov, V.V.; Zaikovskii, V.I.; Malishev, M.E.; Romannikov, V.N. A New Mesoporous Titanium-Silicate Ti-MMM-2: A Highly Active and Hydrothermally Stable Catalyst for H_2O_2-Based Selective Oxidations. *Catal. Today* **2004**, *91–92*, 205–209. https://doi.org/10.1016/j.cattod.2004.03.034.
20. Xiao, F.-S. Ordered Mesoporous Materials with Improved Stability and Catalytic Activity. *Topics Catal.* **2005**, *35*, 9–24. https://doi.org/10.1007/s11244-005-3809-1.

21. Sorokin, A.B.; Tuel, A. Metallophthalocyanine Functionalized Silicas: Catalysts for the Selective Oxidation of Aromatic Compounds. *Catal. Today* **2000**, *57*, 45–59. https://doi.org/10.1016/S0920-5861(99)00312-0.
22. Xiao, F.S.; Han, Y.; Yu, Y., Meng, X.; Yang, M.; Wu, S. Hydrothermally Stable Ordered Mesoporous Titanosilicates with Highly Active Catalytic Sites. *J. Am. Chem. Soc.* **2002**, *124*, 888–889. https://doi.org/10.1021/ja0170044.
23. Wu, P.; Tatsumi, T.; Komatsu, T.; Yashima, T. Postsynthesis, Characterization, and Catalytic Properties in Alkene Epoxidation of Hydrothermally Stable Mesoporous Ti-SBA-15. *Chem. Mater*. **2002**, *14*, 1657–1664. https://doi.org/10.1021/cm010910v.
24. Moliner, M.; Corma, A. Advances in the Synthesis of Titanosilicates: From the Medium Pore TS-1 Zeolite to Highly-Accessible Ordered Materials. *Micropor. Mesopor. Mater*. **2014**, *189*, 31–40. https://doi.org/10.1016/j.micromeso.2013.08.003.
25. Guidotti, M.; Gavrilova, E.; Galarneau, A.; Coq, B.; Psaro, R.; Ravasio, N. Epoxidation of Methyl Oleate with Hydrogen Peroxide. The Use of Ti-Containing Silica Solids as Efficient Heterogeneous Catalysts. *Green Chem.* **2011**, *13*, 1806–1811. https://doi.org/10.1039/C1GC15151G.
26. Guidotti, M.; Pirovano, C.; Ravasio, N.; Lázaro, B.; Fraile, J.M.; Mayoral, J.A.; Coq, B.; Galarneau, A. The Use of H_2O_2 Over Titanium-Grafted Mesoporous Silica Catalysts: A Step Further Towards Sustainable Epoxidation. *Green Chem.* **2009**, *11*, 1421–1427. https://doi.org/10.1039/B903302E.
27. Ivanchikova, I.D.; Kovalev, M.K.; Mel'gunov, M.S.; Shmakov, A.N.; Kholdeeva. O.A. User-Friendly Synthesis of Highly Selective and Recyclable Mesostructured Titanium-Silicate Catalysts for the Production of Bulky Benzoquinones. *Catal. Sci. Technol*. **2014**, *4*, 200–207. https://doi.org/10.1039/C3CY00615H.
28. Ziolek, M. Niobium-Containing Catalysts—The State of the Art. *Catal. Today* **2003**, *78*, 47–64. https://doi.org/10.1016/S0920-5861(02)00340-1.
29. Aronne, A.; Turco, M.; Bagnasco, G.; Ramis, G.; Santacesaria, E.; Di Serio, M.; Marenna, E.; Bevilacqua, M.; Cammarano, C.; Fanelli, E. Gel Derived Niobium–Silicon Mixed Oxides: Characterization and Catalytic Activity for Cyclooctene Epoxidation. *Appl. Catal. A General* **2008**, *347*, 179–185. https://doi.org/10.1016/j.apcata.2008.06.011.
30. Gallo, A.; Tiozzo, C.; Psaro, R.; Carniato, F.; Guidotti, M. Niobium Metallocenes Deposited onto Mesoporous Silica via Dry Impregnation as Catalysts for Selective Epoxidation of Alkenes. *J. Catal*. **2013**, *298*, 77–83. https://doi.org/10.1016/j.jcat.2012.11.015.
31. Ramanathan, A.; Maheswari, R.; Subramaniam, B. Facile Styrene Epoxidation with H_2O_2 over Novel Niobium Containing Cage Type Mesoporous Silicate, Nb-KIT-5. *Top. Catal.* **2015**, *58*, 314–324. https://doi.org/10.1007/s11244-015-0372-2.
32. Ivanchikova, I.D.; Maksimchuk, N.V.; Skobelev, I.Y.; Kaichev, V.V.; Kholdeeva, O.A. Mesoporous Niobium–Silicates Prepared by Evaporation–Induced Self–Assembly as Catalysts for Selective Oxidations with Aqueous H_2O_2. *J. Catal*. **2015**, *332*, 138–148. https://doi.org/10.1016/j.jcat.2015.10.003.
33. Hajjami, N.E.; Thompson, A.B.; Notestein, J.M. Periodic Trends in Highly Dispersed Groups IV and V Supported Metal Oxide Catalysts for Alkene Epoxidation with H_2O_2. *ACS Catal*. **2015**, *5*, 5077–5088. https://doi.org/10.1021/acscatal.5b01105.
34. Kholdeeva, O.A.; Ivanchikova, I.D.; Maksimchuk, N.V.; Skobelev, I.Y. H_2O_2-Based Selective Oxidations: Nb(V) versus Ti(IV). *Catal. Today* **2019**, *333*, 63–70. https://doi.org/10.1016/j.cattod.2018.04.002.
35. Zhang, Z.; Suo, J.; Zhang, X.; Li, S. Synthesis of Highly Active Tungsten-Containing MCM-41 Mesoporous Molecular, Sieve Catalyst. *Chem. Commun.* **1998**, *2*, 241–242. https://doi.org/10.1039/A706719D.
36. Brégeault, J.-M.; Piquemal, J.-Y.; Briot, E.; Duprey, E.; Launay, F.; Salles, L.; Vennat, M.; Legrand, A.-P. New Approaches to Anchoring or Inserting Highly Dispersed Tungsten Oxo (Peroxo) Species in Mesoporous Silicates. *Micropor. Mesopor. Mater*. **2001**, *44–45*, 409–417. https://doi.org/10.1016/S1387-1811(01)00215-3.
37. Dai, W.-L.; Chen, H.; Cao, Y.; Li, H.; Xie, S.; Fan, K. Novel Economic and Green Approach to the Synthesis of Highly Active W-MCM41 Catalyst in Oxidative Cleavage of Cyclopentene. *Chem. Commun.* **2003**, *7*, 892–893. https://doi.org/10.1039/B211666A.
38. Gao, R.; Yanga, X.; Dai, W.-L.; Le, Y.; Li, H.; Fan, K. High-Activity, Single-Site Mesoporous WO_3-MCF Materials for the Catalytic Epoxidation of Cycloocta-1,5-diene with Aqueous Hydrogen Peroxide. *J. Catal.* **2008**, *256*, 259–267. https://doi.org/10.1016/j.jcat.2008.03.017.
39. Yan, W.; Ramanathan, A.; Ghanta, M.; Subramaniam, B. Towards Highly Selective Ethylene Epoxidation Catalysts Using Hydrogen Peroxide and Tungsten- or Niobium-Incorporated Mesoporous Silicate (KIT-6). *Catal. Sci. Technol.* **2014**, *4*, 4433–4439. https://doi.org/10.1039/C4CY00877D.
40. Maksimchuk, N.V.; Ivanchikova, I.D.; Zalomaeva, O.V.; Skobelev, I.Y.; Chesalov, Yu.A.; Shmakov, A.A.; Kholdeeva, O.A. Tungsten-Incorporated Mesoporous Silicate W-MMM-E as Heterogeneous Catalyst for Liquid-Phase Oxidations with Aqueous H_2O_2. *Catalysts* **2018**, *8*, 95–115. https://doi.org/10.3390/catal8030095.
41. Ten Dam, J.; Badloe, D.; Ramanathan, A.; Djanashvili, K.; Kapteijn, F.; Hanefeld, U. Synthesis, Characterisation and Catalytic Performance of a Mesoporous Tungsten Silicate: W-TUD-1. *Appl. Catal. A General* **2013**, *468*, 150–159. https://doi.org/10.1016/j.apcata.2013.08.025.
42. Gontier, S.; Tuel, A. Novel Zirconium Containing Mesoporous SIlicas for Oxidation Reactions in the liquid Phase. *Appl. Catal. A Gen.* **1996**, *143*, 125–135. https://doi.org/10.1016/0926-860X(96)00075-0.
43. Besson, M.; Bonnet, M.C.; Gallezot, P.; Tkatchenko, I.; Tuel, A. Catalysis for Fine Chemicals: Towards Specificity with Polyphasic Media. *Catal. Today* **1999**, *51*, 547–560. https://doi.org/10.1016/S0920-5861(99)00040-1.
44. Morey, M.S.; Stucky, G.D.; Schwarz, S.; Fröba, M. Isomorphic Substitution and Postsynthesis Incorporation of Zirconium into MCM-48 Mesoporous Silica. *J. Phys. Chem. B* **1999**, *103*, 2037–2041. https://doi.org/10.1021/jp980844t.

45. Palazzi, C.; Oliva, L.; Signoretto, M.; Strukul, G. Microporous Zirconia–Silica Mixed Oxides Made by Sol–Gel as Catalysts for the Liquid-Phase Oxidation of Olefins with Hydrogen Peroxide. *J. Catal.* **2000**, *194*, 286–293. https://doi.org/10.1006/jcat.2000.2916.
46. Morandin, M.; Gavagnin, R.; Pinna, F.; Strukul, G. Oxidation of Cyclohexene with Hydrogen Peroxide Using Zirconia–Silica Mixed Oxides: Control of the Surface Hydrophilicity and Influence on the Activity of the Catalyst and Hydrogen Peroxide Efficiency. *J. Catal.* **2002**, *212*, 193–200. https://doi.org/10.1006/jcat.2002.3782.
47. Maksimchuk, N.V.; Melgunov, M.S.; Mrowiec-Białoń, J.; Jarzębski, A.B.; Kholdeeva, O.A. H_2O_2-Based Allylic Oxidation of α-Pinene over Different Single Site Catalysts. *J. Catal.* **2005**, *235*, 175–183. https://doi.org/10.1016/j.jcat.2005.08.001.
48. Chaudhari, K.; Bal, R.; Srinivas, D.; Chandwadkar, A.J.; Sivasanker, S. Redox Behavior and Selective Oxidation Properties of Mesoporous Titano- and Zirconosilicate MCM-41 Molecular Sieves. *Microporous Mesoporous Mater.* **2001**, *50*, 209–218. https://doi.org/10.1016/S1387-1811(01)00454-1.
49. Liu, J.M.; Liao, S.J.; Jiang, G.D.; Zhang, X.L.; Petrik, L. Preparation, Characterization and Catalytic Activity of Zr Embedded MSU-V with High Thermal and Hydrothermal Stability. *Microporous Mesoporous Mater.* **2006**, *95*, 306–311. https://doi.org/10.1016/j.micromeso.2006.06.003.
50. Quignard, F.; Choplin, A.; Teissier, R. A Molecular Route Towards Silica Supported Zirconium Catalysts Active for the Mild Oxidation of Olefins with H_2O_2. *J. Mol. Catal. A Chem.* **1997**, *120*, L27–L31. https://doi.org/10.1016/S1381-1169(97)00031-9.
51. Thornburg, N.E.; Notestein, J.M. Rate and Selectivity Control in Thioether and Alkene Oxidation with H_2O_2 over Phosphonate-Modified Niobium(V)–Silica Catalysts. *ChemCatChem* **2017**, *9*, 3714–3724. https://doi.org/10.1002/cctc.201700526.
52. Maksimchuk, N.V.; Evtushok, V.Y.; Zalomaeva, O.V.; Maksimov, G.M.; Ivanchikova, I.D.; Chesalov, Y.A.; Eltsov, I.V.; Abramov, P.A.; Glazneva, T.S.; Yanshole, V.V.; et al. Activation of H_2O_2 over Zr(IV). Insights from Model Studies on Zr-Monosubstituted Lindqvist Tungstates. *ACS Catal.* **2021**, *11*, 10589–10603. https://doi.org/10.1021/acscatal.1c02485.
53. Maksimchuk, N.V.; Ivanchikova, I.D.; Cho, K.H.; Zalomaeva, O.V.; Evtushok, V.Yu.; Larionov, K.P.; Glazneva, T.S.; Chang, J.-S.; Kholdeeva, O.A. Catalytic Performance of Zr-Based Metal-Organic Frameworks Zr-abtc and MIP-200 in Selective Oxidations with H_2O_2. *Chem. Eur. J.* **2021**, *27*, 6985–6992. https://doi.org/10.1002/chem.202005152.
54. Kholdeeva, O.A.; Maksimchuk, N.V. Metal-Organic Frameworks in Oxidation Catalysis with H_2O_2. *Catalysts* **2021**, *11*, 283. https://doi.org/10.3390/catal11020283.
55. Jaenicke, S.; Loh, W.L. Preparation of highly dispersed molybdenum on alumina by thermal decomposition of $Mo(CO)_6$. *Catal. Today* **1999**, *49*, 123–130. https://doi.org/10.1016/S0920-5861(98)00416-7.
56. Debecker, D.P.; Stoyanova, M.; Rodemerck, U.; Eloy, P.; Leonard, A.; Su, B.L.; Gaigneaux, E.M. Thermal Spreading As an Alternative for the Wet Impregnation Method: Advantages and Downsides in the Preparation of $MoO_3/SiO_2{-}Al_2O_3$ Metathesis Catalysts. *J. Phys. Chem. C* **2010**, *114*, 18664–18673. https://doi.org/10.1021/jp1074994.
57. Tiozzo, C.; Bisio, C.; Carniato, F.; Marchese, L.; Gallo, A.; Ravasio, N.; Psaro, R.; Guidotti, M. Epoxidation with Hydrogen Peroxide of Unsaturated Fatty Acid Methyl Esters over Nb(V)-Silica Catalysts. *Eur. J. Lipid Sci. Technol*. **2013**, *115*, 86–93. https://doi.org/10.1002/ejlt.201200217.
58. Nielsen, R.H.; Schlewitz, J.H.; Nielsen, H. Zirconium and Zirconium Compounds. In *Kirk-Othmer Encyclopedia of Chemical Technology*; John Wiley & Sons, Inc.: Hoboken, NJ, USA, 2013. https://doi.org/10.1002/0471238961.26091803.a01.pub3.
59. Schubert, U. Chemical Modification of Titanium Alkoxides for Sol–Gel Processing. *J. Mater. Chem.* **2005**, *15*, 3701–3715. https://doi.org/10.1039/B504269K.
60. Tuel, A.; Gontier, S.; Teissier, R. Zirconium Containing Mesoporous Silicas: New Catalysts for Oxidation Reactions in the Liquid Phase. *Chem. Commun. 1996*, 651–652. https://doi.org/10.1039/CC9960000651.
61. El Haskouri, J.; Cabrera, S.; Guillem, C.; Latorre, J.; Beltrán, A.; Beltrán, D.; Marcos, M.D.; Amorós, P. Atrane Precursors in the One-Pot Surfactant-Assisted Synthesis of High Zirconium Content Porous Silicas. *Chem. Mater.* **2002**, *14*, 5015–5022. https://doi.org/10.1021/cm020131u.
62. Newalkar, B.L.; Olanrewaju, J.; Komarneni, S. Microwave-Hydrothermal Synthesis and Characterization of Zirconium Substituted SBA-15 Mesoporous Silica. *J. Phys. Chem. B* **2001**, *105*, 8356–8360. https://doi.org/10.1021/jp010889l.
63. Ramanathan, A.; Castro Villalobos, M.; Kwakernaak, C.; Telalovic, S.; Hanefeld, U. Zr-TUD-1: A Lewis Acidic, Three-Dimensional, Mesoporous, Zirconium-Containing Catalyst. *Chem.–Eur. J.* **2008**, *14*, 961–972. https://doi.org/10.1002/chem.200700725.
64. Zhu, H.; Maheswari, R.; Ramanathan, A.; Subramaniam, B. Evaporation-Induced Self-Assembly of Mesoporous Zirconium Silicates with Tunable Acidity and Facile Catalytic Dehydration Activity. *Microporous Mesoporous Mater.* **2016**, *223*, 46–52. https://doi.org/10.1016/j.micromeso.2015.10.026.
65. Barberis, P.; Merle-Méjean, T.; Quintard, P. On Raman Spectroscopy of Zirconium Oxide Films. *J. Nucl. Mater.* **1997**, *246*, 232–243. https://doi.org/10.1016/S0022-3115(97)00038-X.
66. Kontoyannis, C.G.; Orkoula, M. Quantitative Determination of the Cubic, Tetragonal and Monoclinic Phases in Partially Stabilized Zirconias by Raman Spectroscopy. *J. Mater. Sci.* **1994**, *29*, 5316–5320. https://doi.org/10.1007/BF01171541.
67. Morrow, B.A.; McFarlan, A.J. Infrared and Gravimetric Study of an Aerosil and a Precipitated Silica using Chemical and Hydrogen/Deuterium Exchange Probes. *Langmuir* **1991**, *7*, 1695–1701. https://doi.org/10.1021/la00056a022.
68. Miller, J.B.; Ko, E.I. Acidic Properties of Silica-Containing Mixed Oxide Aerogels: Preparation and Characterization of Zirconia–Silica and Comparison to Titania–Silica. *J. Catal.* **1996**, *159*, 58–68. https://doi.org/10.1006/jcat.1996.0064.
69. Flego, C.; Carluccio, L.; Rizzo, C.; Perego, C. Synthesis of Mesoporous SiO_2–ZrO_2 Mixed Oxides by Sol–Gel Method. *Catal. Commun.* **2001**, *2*, 43–48. https://doi.org/10.1016/S1566-7367(01)00006-1.

70. Hadjiivanov, K.; Lavalley, J.C. FT–IR Spectroscopic Study of CO Adsorption on Monoclinic Zirconia of Different Hydroxylation Degrees. *Catal. Commun.* **2001**, *2*, 129–133. https://doi.org/10.1016/S1566-7367(01)00020-6.
71. Morterra, C.; Cerrato, G.; Di Ciero, S. IR Study of the Low Temperature Adsorption of CO on Tetragonal Zirconia and Sulfated Tetragonal Zirconia. *Appl. Surf. Sci.* **1998**, *126*, 107–128. https://doi.org/10.1016/S0169-4332(97)00581-3.
72. Paukshtis, E.A.; Yurchenko, E.N. Study of the Acid–Base Properties of Heterogeneous Catalysts by Infrared Spectroscopy. *Russ. Chem. Rev*. **1983**, *52*, 242–258. https://doi.org/10.1070/RC1983v052n03ABEH002812.
73. Trukhan, N.N.; Panchenko, A.A.; Roduner, E.; Melgunov, M.S.; Kholdeeva, O.A.; Mrowiec-Bialon, J., Jarzebski, A.B. FTIR Spectroscopic Study of Titanium-Containing Mesoporous Silicate Materials. *Langmuir* **2005**, *21*, 10545–10554. https://doi.org/10.1021/la0514516.
74. Zecchina, A.; Bordiga, S.; Spoto, G.; Marchese, I.; Petrini, G.; Leofanti, G.; Padovan, M. Silicalite Characterization. 2. IR Spectroscopy of the Interaction of Carbon Monoxide with Internal and External Hydroxyl Groups. *J. Phys. Chem.* **1992**, *96*, 4991–4997.
75. Yamaguchi, T.; Morita, T.; Salama, T.M.; Tanabe, K. *Catal. Lett*. **1990**, *4*, 1–6. https://doi.org/10.1007/BF00764864.
76. Chen, L.F.; Zhou, X.L.; Norena, L.E.; Wang, J.A.; Navarrete, J.; Salas, P.; Montoya, A.; Del Angel, P.; Llanos, M.E. Comparative Studies of Zr-Based MCM-41 and MCM-48 Mesoporous Molecular Sieves: Synthesis and Physicochemical Properties. *Appl. Surf. Sci.* **2006**, *253*, 2443–2451. https://doi.org/10.1016/j.apsusc.2006.04.064.
77. Ramanathan, A.; Subramaniam, B.; Maheswari, R.; Hanefeld, U. Synthesis and Characterization of Zirconium Incorporated Ultra Large Pore Mesoporous Silicate, Zr–KIT-6. *Micropor. Mesopor. Mater.* **2013**, *167*, 207–212. https://doi.org/10.1016/j.micromeso.2012.09.008.
78. Vasudevan, S.V.; Cai, J.; Bu, Q.; Mao, H. Ordered Mesoporous Zirconium Silicates as a Catalyst for Biofuel Precursors Synthesis. *Mol. Catal.* **2021**, *516*, 112003. https://doi.org/10.1016/j.mcat.2021.112003.
79. Nash, C.P.; Ramanathan, A.; Ruddy, D.A.; Behl, M.; Gjersing, E.; Griffin, M.; Zhu, H.; Subramaniam, B.; Schaidle, J.A.; Hensley, J.E. Mixed Alcohol Dehydration over Brønsted and Lewis Acidic Catalysts. *Appl. Catal. A: General* **2016**, *510*, 110–124. https://doi.org/10.1016/j.apcata.2015.11.019.
80. Ivanchikova, I.D.; Skobelev, I.Y.; Maksimchuk, N.V.; Paukshtis, E.A.; Shashkov, M.V.; Kholdeeva, O.A. Toward Understanding the Unusual Reactivity of Mesoporous Niobium Silicates in Epoxidation of C=C Bonds with Hydrogen Peroxide. *J. Catal.* **2017**, *356*, 85–99. https://doi.org/10.1016/j.jcat.2017.09.011.
81. Soltanov, R.I.; Paukshtis, E.A.; Yurchenko, E.N. IK-Study of Thermodynamic Characteristics of Carbon Monoxide Interaction with the Surface of Some Oxide Adsorbents. *Kinet. Catal.* **1982**, *23*, 164–170.
82. Zalomaeva, O.V.; Evtushok, V.Yu.; Ivanchikova, I.D.; Glazneva, T.S.; Chesalov, Yu.A.; Larionov, K.P.; Skobelev, I.Y.; Kholdeeva, O.A. Nucleophilic versus Electrophilic Activation of Hydrogen Peroxide over Zr-Based Metal–Organic Frameworks. *Inorg. Chem.* **2020**, *59*, 10634–10649. https://doi.org/10.1021/acs.inorgchem.0c01084.
83. Paukshtis, E.A.; Kotsarenko, N.S.; Karakchiev, L.G. Investigation of Proton-Acceptor Properties of Oxide Surfaces by IR Spectroscopy of Hydrogen-Bonded Complexes. *React. Kinet. Catal. Lett.* **1979**, *12*, 315–319. https://doi.org/10.1007/BF02064262.
84. Paukshtis, E.A. *Infrared Spectroscopy in Heterogeneous Acid–Base Catalysis*; Novosibirsk: Nauka, Russia, 1992; 253p. (In Russian)
85. Sheldon, R.A.; Kochi, J.K. *Metal–Catalyzed Oxidations of Organic Compounds*; Academic Press: New York, NY, USA, 1981; 446p. https://doi.org/10.1016/B978-0-12-639380-4.X5001-5.
86. Maksimchuk, N.V.; Lee, J.S.; Solovyeva, M.V.; Cho, K.H.; Shmakov, A.N.; Chesalov, Y.A.; Chang, J.-S.; Kholdeeva, O.A. Protons Make Possible Heterolytic Activation of Hydrogen Peroxide over Zr-Based Metal-Organic Frameworks. *ACS Catal.* **2019**, *9*, 9699–9704. https://doi.org/10.1021/acscatal.9b02941.
87. Van Sickle, D.E.; Mayo, F.R.; Arluck, R.M. Liquid-Phase Oxidations of Cyclic Alkenes. *J. Amer. Chem. Soc.* **1965**, *87*, 4824–4832. https://doi.org/10.1021/ja00949a028.
88. Botar, B.; Geletii, Yu.V.; Kögerler, P.; Musaev, D.G.; Morokuma, K.; Weinstock, I.A.; Hill, C.L. The True Nature of the Di-iron(III) γ-Keggin Structure in Water: Catalytic Aerobic Oxidation and Chemistry of an Unsymmetrical Trimer. *J. Amer. Chem. Soc.* **2006**, *128*, 11268–11277. https://doi.org/10.1021/ja063157l.
89. Food Drug Administration. Rules and Regulations: Title 21—Food and Drugs, Food Additives, Synthetic Flavoring Substances and Adjuvants. *Fed Regist* **1973**, *95*, 12913.
90. Bauer, K.; Garbe, D.; Surburg, H. *Common Fragrance and Flavor Materials*; Wiley-VCH: New York, NY, USA, 1997; 278p.
91. Guidotti, M. *Institute CNR-ISTM Internal Report*; CNR-ISTM: Milan, Italy, 2018.
92. Di Furia, F.; Modena, G. Mechanism of Oxygen Transfer from Peroxo Species. *Pure Appl. Chem.* **1982**, *54*, 1853–1866. https://doi.org/10.1351/pac198254101853.